Isotope geochemistry of Proterozoic talc occurrences in Archean marbles of the Ruby Mountains, southwest Montana, U.S.A.

**John B. Brady[1], John T. Cheney[2], Amy Larson Rhodes[1]
Angela Vasquez[2], Chris Green[2], Mathieu Duvall[3], Ari Kogut[4]
Lewis Kaufman[5], Dana Kovaric[1]**

Departments of Geology: [1]Smith College, Northampton, MA 01063 (jbrady@science.smith.edu)
[2]Amherst College, Amherst, MA, [3]Colorado College, Colorado Springs, CO
[4]Beloit College, Beloit, WI, [5]College of Wooster, Wooster, OH
(Received July 15, 1998; Published December 31, 1998)

Abstract

Talc occurs as massive, economic deposits in upper amphibolite facies marbles of Archean age in southwestern Montana. Previous workers have demonstrated that the talc is a replacement of the marble that resulted from interaction with a large volume of fluid. $\delta^{18}O$ (SMOW) values for dolomite and calcite range from 20-25‰ for the unaltered Archean marbles to as little as 8-10‰ in the talc deposits, suggesting that the metasomatic fluids had low $\delta^{18}O$ values. In contrast, $\delta^{13}C$ values for calcite and dolomite are similar for all samples (-2 to +2‰ PDB). Therefore, it is likely that the metasomatic fluids were oxygen-rich and carbon-poor, namely water-rich and CO_2-poor. A CO_2-poor fluid is also indicated by $\Delta^{13}C$ (calcite-graphite) values (3.6-5.3‰), which appear little altered from values expected for upper amphibolite facies marbles, and by the occurrence of the mineral assemblage talc+calcite. $^{40}Ar/^{39}Ar$ age spectra for hornblende, phlogopite, and biotite record cooling at 1.72 Ga from a regional thermal event. $^{40}Ar/^{39}Ar$ age spectra of fine-grained muscovite associated with the talc date talc formation at 1.36 Ga. The Ar data limit the temperature of talc crystallization to below ~350°C, the biotite closure temperature for Ar diffusion. If the metasomatic fluid was seawater (0‰), then the carbonate oxygen data require a minimum temperature of 270°C for talc formation. Oxygen ($\delta^{18}O$ = 4.7 to 8.8 ‰) and hydrogen (D/H = -49.9 to -57.6 SMOW) isotope data for the talc are consistent with a 200°-300°C metasomatic fluid derived from seawater, based on theoretical models of the fractionation of oxygen and hydrogen between talc and water. Regional, northwest-trending faults associated with the extension that formed the Belt Basin in the Middle Proterozoic may have provided channels for seawater to circulate in continental crust and to react with marble, forming talc at depths of 5-10 km.

Keywords: talc, oxygen, carbon, hydrogen, argon, isotopes, Proterozoic, metasomatic, dolomite, calcite, graphite, chlorite, Montana

Introduction

Talc has been mined in southwest Montana for over fifty years (Olson, 1976) and several major talc mines were in operation in the 1990's. Olson (1976) and Berg (1979) described and catalogued some 50 talc occurrences in the Ruby and nearby Gravelly, Snow Crest, Owl Creek, Highland, and Tobacco Root ranges. Mining of talc in the area is economic because of the very high purity and large extent of the deposits. Ore zones that are virtually 100% talc can be traced for several hundred meters along strike. The talc deposits are confined stratigraphically to marble units in an Archean metasedimentary sequence and previous workers (Okuma, 1971; Garihan, 1973; Olson, 1976; Berg, 1979; Anderson et al., 1990) have concluded that the talc formed by a metasomatic replacement of the marble. The scale of the talc occurrences, the significant chemical difference between pure talc and the Archean marble host, and the small number of minerals present in most samples suggest that a large scale fluid flow system led to the formation of the deposits. In this paper we present new petrologic, geochemical, and geochronological data that constrain the physical conditions and timing of talc formation. We believe our data support a model of talc formation as a result of circulation of seawater through continental crust along faults during a Middle Proterozoic extensional event.

Regional geology

The Ruby Mountains are one of a group of Archean-cored, block-faulted mountain ranges that dominate southwest Montana. A structurally complex region of Paleozoic and Mesozoic rocks occupies the relatively inaccessible northern portion of the range, but most of the Ruby Mountains are highly-deformed Archean metasedimentary and metaigneous rocks (Figure 1). Geologic maps are available for much of the range due to the careful work of Okuma (1971), Garihan (1973), Tysdal (1976), Karasevich et al. (1981), and James (1990). Most of the talc occurs in the western half of the Ruby Range in marbles of the Christensen Ranch Metasedimentary Suite (James, 1990), which also includes quartzofeldspathic gneiss, sillimanite schist, banded iron formation, and anthophyllite gneiss. East of the metasedimentary sequence is a thick quartzofeldspathic gneiss ("Dillon Granite Gneiss") that has been described as an intrusive rock by many, but the protolith of this gneiss is a matter of debate (Karasevich et al., 1981). Still farther east is a possibly older suite of metamorphic rocks that is generally lacking in marbles and, therefore, lacking in talc deposits. Serpentinized ultramafic rocks occur among the "older gneisses" in the southeastern part of the range, but are not spatially associated with the major talc deposits (Desmarais, 1981).

Geochronology and metamorphism

The Archean rocks were deformed and metamorphosed to upper amphibolite facies conditions, probably at one or more of the following times: 3.3, 2.7, 2.4 or 1.8 Ga (see below). Based on mineral assemblage thermobarometry, Dahl (1979, 1980) determined that peak metamorphic conditions were 675°-745°C and 0.5-0.8 GPa. We observed migmatite zones in some gneisses, that we interpret as evidence for partial melting during metamorphism. The marbles developed a coarse texture and the mineral assemblage calcite-diopside-forsterite-phlogopite-graphite. Many of the Archean metamorphic rocks of the Ruby and nearby ranges have a patchy overprint of greenschist facies mineral assemblages. Whether this retrograde metamorphic overprint developed during cooling from upper amphibolite conditions or during some later period of regional heating

is not yet known. Because they observed talc replacing the greenschist minerals serpentine and tremolite, Anderson et al. (1990) believe that the greenschist overprint predates the talc deposits.

The upper amphibolite facies metamorphism has long been believed to have occurred at about 2.7 Ga. This age is based on Rb-Sr dating of gneiss samples from the Ruby Range by James and Hedge (1980) and from the Tobacco Root Mountains by Mueller and Cordua (1976) and is consistent with ages determined for Archean rocks in nearby ranges of the Wyoming Province (Wooden et al., 1988). However, recently Mueller and Mogk (personal communication) have found detrital zircons in similar metasedimentary rocks of the adjacent Tobacco Root Mountains that have metamorphic (overgrowth) ages of 3.3 Ga and core (detrital?) ages of up to 3.9 Ga. Krogh and Hess (1997) have dated a metamorphic zircon from the Tobacco Root mountains at 2.4 Ga, which is consistent with the U-Pb systematics of zircons found in the 75 Ma Tobacco Root batholith by Mueller et al. (1997). O'Neill et al. (1988) have reported ages of 1.8 Ga for zircon which they believe grew during an upper amphibolite facies metamorphism of the Highland Mountains northwest of the Ruby Range. Giletti (1966) obtained K-Ar and Rb-Sr ages of 1.4 to 1.7 Ga on minerals and rocks of the Ruby Range and concluded that there was a 1.6 Ga Proterozoic thermal event that reset the isotopic clocks. Although Giletti analyzed fresh rocks, James (1990) and others have postulated that the 1.6 Ga date coincides with the widespread development of scattered greenschist facies mineral assemblages. A number of workers have also suggested that talc formation was associated with this thermal event (for example, Berg, 1979). Brady et al. (1994) and Kovaric et al. (1996) report $^{40}Ar/^{39}Ar$ ages of 1.7 Ga for hornblende and biotite from the Tobacco Root Mountains northeast of the Ruby Range. If the Ruby Range also experienced upper amphibolite facies conditions at 1.7-1.8 Ga, then perhaps Giletti's 1.6 Ga K-Ar ages mark cooling from a 1.7 Ga metamorphism.

The Ruby Range is crosscut by a series of NW-trending faults that clearly offset the Christensen Ranch Metasedimentary Suite (Figure 1). Faults with the same trend are common in the surrounding ranges as well (for example, Vitaliano et al., 1979). Some of the talc deposits appear to be associated with the NW-trending faults (Garihan, 1973) and their origin, therefore, may post-date at least some of the movement along these faults. Schmidt and Garihan (1986) have demonstrated repeated movement along these faults beginning in Middle Proterozoic time. Two groups of unmetamorphosed diabase dikes, dated by Rb-Sr at 1.1 and 1.4 Ga (Wooden et al., 1978), are widespread in the region. These dikes typically have a NW-trend and a few follow directly the trace of NW-trending faults. Therefore, it appears that the diabase dikes post-date the initiation of movement along the NW-trending faults. Regionally, these faults and the associated diabase dikes have been attributed to the crustal extension that created the Belt Basin beginning at about 1.4 Ga (Wooden et al., 1978; Schmidt and Garihan, 1986).

Constraints on talc formation

Previous work on Ruby Range talc by Okuma (1971), Garihan (1973, 1976), Olson (1976), Berg (1979), Dahl (1979, 1980), and Anderson et al. (1990) established a number of important constraints on the origin of the talc deposits. (1) Talc occurs only within the boundaries of highly-folded and metamorphosed Precambrian marble units and not within nearby limestones of Cambrian or younger age. Formation of the talc deposits is believed, therefore, to have occurred during Precambrian time. (2) Some of the larger talc deposits are associated with structural features

such as NW-trending regional faults and the hinge regions of major folds (Garihan, 1973; Okuma, 1971). Formation of the talc deposits is believed, therefore, to have occurred after the formation of these folds and faults. (3) Mineral assemblages in metamorphic rocks near to, but not affected by, talc formation record upper amphibolite facies conditions of 675° to 745°C and pressures of 0.5-0.8 GPa (Dahl, 1979, 1980). Observed talc-carbonate assemblages are not compatible with these conditions, so the talc must have crystallized at lower temperatures after the peak metamorphic conditions were attained. (4) Although the marbles near the talc occurrences are principally dolomite, in some cases the same marble layers at a distance from the talc occurrences are largely calcite (Anderson et al., 1990). Based on this finding, Anderson et al. (1990) proposed that formation of the talc deposits began with the hydrothermal dolomitization of largely calcite marbles. A similar concentration of dolomite in the vicinity of talc deposits in marble was observed in Bavaria by Stettner (1959). (5) Significant metasomatism is required to transform a largely calcite marble to a massive, monomineralic talc body. The scale (tens of meters across strike) and monomineralic character of the talc deposits require a fluid-dominated chemical system to accomplish the evident mass transfer (Korzhinskii, 1970). (6) Gneisses interbedded with talc-replaced marbles have been largely altered to chlorite (clinochlore). The effect of the metasomatic fluids depended to some extent on the protolith.

Talc samples

Field observations

During the summer of 1990 we sampled extensively a number of talc deposits in the Ruby Range for petrologic and geochemical study using Olson's (1976) and Berg's (1979) reports and maps by James (1990), Anderson (1987), J.F. Childs (unpublished map), and D. Van Alstine (unpublished map) as field guides. No new mapping was undertaken. Field and laboratory data were collected for eight of the talc occurrences shown on Figure 1. Particularly detailed studies were completed on the Regal-Keystone mine and on the American Chemet mine. Our field observations were largely consistent with those of previous workers. Talc occurs as veins and pods within and as massive replacements of folded marble layers. In most cases, there is no obvious control on the location of the talc visible in the field, except that it is within the marble. Whatever the plumbing plan may have been for the metasomatic fluids, it was certainly complex (Figure 2). We were particularly puzzled by the seemingly unconnected pods of talc, some of which may be cross sections of fluid-flow channels. In a few instances, talc appeared to be more abundant along the boundaries of the marble with adjacent units, as if the layer boundaries provided good fluid pathways.

Talc has replaced dolomite with little apparent change in volume. In some cases bedding in the marble can be traced across talc veins without obvious deflection. Based on textures such as these, Anderson et al. (1990) argue for a constant volume process in a rigid crust above the brittle/ductile transition. Pseudomorphs of polycrystalline talc after single crystals of dolomite can be found (Figures 3, 4). In thin section the talc textures are complex, but talc consuming dolomite is the most common observation (Figures 5-7). Sharp contacts between talc and carbonate are common. Talc replaces carbonate crystals along cross-cutting veins and along simple or irregular contacts that may be boundaries to larger veins. Although the carbonate in most talc rocks is dolomite, some contain calcite as well. Textures consistent with late calcite (post-dolomite) and textures consistent with early calcite (pre-dolomite) were observed. Talc crystals vary in size from a few

microns or less to several millimeters. We could find no consistent pattern for the occurrence of coarse- versus fine-grained talc crystals. In many cases, coarse talc was separated from carbonate by fine-grained talc, but this is not always the case. We believe that the coarse talc crystals were not the result of some initial marble texture, but rather due to variations in nucleation, growth, or coarsening during talc formation. See Anderson et al. (1990) for additional petrographic details and photomicrographs.

Mineral assemblages and reactions

Typical mineral assemblages of the talc deposits include talc, talc+dolomite, talc+calcite, talc+chlorite, talc+calcite+quartz, and talc+calcite+chlorite+quartz. At least one location has the assemblage talc+tremolite+calcite. “Fibrous talc” and large (several cm) talc pseudomorphs of tremolite were found at several locations, notably the Smith-Dillon mine, but overall tremolite and tremolite pseudomorphs are rare. Chlorite is present in many of the talc samples. The color of the rock is a rough indicator of the proportion of chlorite, with pure talc rocks being a pale green and chlorite-rich talc rocks being a darker green. In many cases, the chlorite occurs as pseudomorphs of silicate minerals such as phlogopite that were present in the original marble. There is clear textural evidence that chlorite is being replaced by talc in some samples (Figure 8).

Although talc can be produced or consumed by reactions involving dolomite and quartz or tremolite, these reactions cannot have led to the formation of most of the talc in the Ruby Range because neither quartz nor tremolite is common in the host marbles. We believe the talc formed by reaction of calcite with aqueous solutions to produce first dolomite from the calcite, then talc from the dolomite. We observed numerous oval quartz crystals in coarse dolomite marble at several locations near talc bodies (Figure 9). The assemblage dolomite+quartz could not have survived metamorphism to upper amphibolite facies conditions, so dolomite (or quartz) crystallization must postdate this metamorphism. Reactions like the following are envisioned as being principally responsible for the talc deposits:

$$2\ CaCO_3\ (Cal) + Mg^{+2}\ (aq) = CaMg(CO_3)_2\ (Dol) + Ca^{+2}\ (aq) \qquad (1)$$

$$3\ CaMg(CO_3)_2\ (Dol) + 3\ Mg^{+2}\ (aq) + 8\ H_4SiO_4 \cdot 2\ H_2O(aq) = 2\ Mg_3Si_4O_{10}(OH)_2\ (Tlc) + 3\ Ca^{+2}\ (aq) + 6\ CO_2 + 30\ H_2O \qquad (2)$$

Except for silica (Walther and Orville, 1983), we do not know the specific aqueous species involved, but we think the important minerals are calcite, dolomite, and talc. Other silicate minerals may participate where they occur, but their role is minor.

Anderson et al. (1990) calculated a volumetric water/rock value of at least 600, based on the amount of silica needed to convert their average Ruby Range marble to pure talc. To convert a pure calcite marble to talc would require minimum volumetric water-rock ratios two to three times higher based on Walther and Orville's (1983) quartz solubility data and temperatures of 300-400°C. Using the Mg content of modern seawater, a minimum volumetric water/rock value of 300-400 is needed to convert calcite to dolomite and a volumetric water/rock value over 500 is needed to convert calcite to talc. Unless fluid-rock equilibrium is attained at all times, the actual water/rock values were probably much higher.

Based on the observed mineral assemblages talc+calcite and talc+dolomite, important constraints on the physical conditions can be obtained from experimental studies. Because both water and carbon dioxide are involved in the talc-forming reactions, the mole fraction of CO_2 in the talc-forming fluids (principally H_2O- CO_2 fluids?) is as important as temperature and pressure. Relevant chemical reactions, modeled with Berman's (1988) thermodynamic data set, are shown as a function of temperature (T) and mole fraction of CO_2 (X(CO2)) in Figure 10 for a pressure of 0.2 GPa. Clear upper limits on temperature (450°C) and mole fraction of CO_2 (0.5) for the assemblage talc+calcite are visible in Figure 10. Unfortunately, useful lower limits for either temperature or mole fraction of CO_2 are not apparent. Based on the large volume of fluid required to form the talc deposits (see p.6), it is likely that the fluid had a low mole fraction of CO_2. At 0.5 GPa (not shown), the temperature limit to the assemblage talc+calcite approaches 500°C, whereas the upper limit to the mole fraction of CO_2 falls to 0.1. We do not have a good constraint on the pressure of talc formation, but pressures as high as 0.5 GPa are inconsistent with the modest temperatures and high volumes of fluid flow believed to be associated with talc formation.

$^{40}Ar/^{39}Ar$ age spectra

Hornblende, biotite, and phlogopite were separated from marbles and amphibolites within and adjacent to several talc deposits. $^{40}Ar/^{39}Ar$ age spectra (Figure 11) were collected for these samples by Dan Lux at the University of Maine following the procedures of Lux et al. (1989). All of the samples give total gas ages in the interval 1650-1750 Ma, consistent with the Proterozoic thermal event identified by the K-Ar data of Giletti (1966), but considerably younger than the Rb-Sr ages (2.7 Ga) of the upper amphibolite facies metamorphism determined by James and Hedge (1980). Plateau ages for all samples are in the interval 1716-1764 Ma, with hornblende and phologopite ages clustered at 1721 Ma. The mica ages are not consistently younger than the amphibole ages, contrary to what is expected for simple regional cooling from minerals with such different closure temperatures. Either the regional cooling was quite rapid or the samples have a thermal history more complex than simple cooling (Hodges et al., 1994). Hornblende $^{40}Ar/^{39}Ar$ age spectra from the Tobacco Root mountains (Kovaric et al., 1996) give similar ages (1700 Ma).

For hornblende to give a plateau age of 1725 Ma, the hornblende crystals must have cooled through the hornblende closure temperature of about 525°C (McDougall and Harrison, 1988) at that time. The observed mineral assemblage talc+calcite is not stable at 525°C at any crustal pressure. Therefore, the talc deposits must have formed **after** 1725 Ma. Because phlogopite and biotite also both give plateau ages in the 1716-1764 Ma interval, it appears that the talc deposits formed after these minerals were last cooled through their closure temperatures (375-325°C, McDougall and Harrison, 1988). It is possible that the talc formed **during** the regional cooling at 1725 Ma, but other evidence suggests that it was formed more recently and is not related to regional metamorphism.

If the talc formed after the Proterozoic thermal event, then it must have formed at temperatures that were not high enough to reset the K-Ar clocks of biotite and phlogopite. Biotite closure temperatures depend on the chemical composition of the biotite as well as the cooling rate and crystal size, with phlogopite having the highest closure temperatures (375°C) and intermediate biotites having lower closure temperatures (325-350°C) (McDougall and Harrison, 1988, p.151). Therefore, the $^{40}Ar/^{39}Ar$ data imply that the talc formed at temperatures below 350°C. Interestingly,

the $^{40}Ar/^{39}Ar$ data for biotites studied are the most disturbed, with two samples not defining plateau ages. This may mean that the temperature of talc formation was close to the closure temperature of biotite, but significantly below the closure temperatures of phlogopite and hornblende.

Quartzofeldspathic gneisses interbedded with talc-replaced marble are altered to magnesium-rich chlorite (clinochlore). Biotite and feldspar in the gneisses are replaced first, yielding a chlorite rock with quartz ribbons (see Anderson et al., 1990, Fig. 9). Further alteration of the gneisses can produce a wholly chlorite rock, or a talc-chlorite rock (see Anderson et al., 1990, Fig. 10). With still further alteration, the chlorite can be replaced by talc. In some cases, gneissic banding can be traced from unaltered gneiss into chlorite bands surrounded by talc. In the transition zone, fine-grained muscovite is also present and we believe from this and other textural evidence that the muscovite was produced at the time of talc formation. Fine-grained (10-50 μm) muscovite separated from altered gneiss collected at the American Chemet mine gave Kovaric et al. (1996) a $^{40}Ar/^{39}Ar$ plateau age of 1363 Ma (Figure 12), which we believe dates the formation of the talc. A 1363 Ma age for the talc deposits is consistent with the field evidence, mentioned above, that links some of the talc occurrences with Middle Proterozoic faulting.

Stable isotopes

Oxygen, carbon, and hydrogen isotopic compositions were determined for samples of calcite, dolomite, talc, and graphite as appropriate from the Ruby Range talc deposits (Larson, 1991; Vasquez, 1991). Carbonate and talc samples were taken from rock samples with a dental drill. The carbonate was identified as calcite or dolomite by staining the chip with alizarin red or by reactivity tests using dilute hydrochloric acid. Graphite was separated from the other minerals by floatation in water. Carbonate minerals were analyzed for ^{18}O and ^{13}C contents at the Dartmouth College stable isotope laboratory by the conventional technique of McCrea (1950). Talc samples were analyzed for ^{18}O at Dartmouth in Ni reaction vessels by the BrF_5 method (Clayton and Mayeda, 1963). Talc samples were analyzed for H_2O and D/H contents at Southern Methodist University by Kurt Ferguson following the procedures of Bigeleisen et al. (1952) as described by Holdaway et al. (1986). Graphite samples were oxidized with excess CuO according to the method outlined by Stern et al. (1992), producing CO_2 for ^{13}C analysis. All of the oxygen data are reported as $\delta^{18}O$ (SMOW), all of the D/H data as D/H (SMOW), and all of the carbon data as $\delta^{13}C$ (PDB) (O'Neil, 1986). Two or more analyses were performed for most samples. Data are shown in the figures as the mean of the analyses for each sample. Error bars are the standard deviation from the mean. Because analytical precision seems is for most samples, the large error bars for some samples are believed to represent sample inhomogeneity rather than analytical error.

Carbonate minerals

$\delta^{18}O$ and $\delta^{13}C$ values for carbonate samples from the Regal-Keystone Mine are shown in Figure 13. The same scale is used for both $\delta^{18}O$ and $\delta^{13}C$ to emphasize the large variation in $\delta^{18}O$ relative to $\delta^{13}C$. Values of $\delta^{18}O$ range from those expected for marbles derived from marine carbonates (20-25‰) (Valley, 1986; Criss, 1995) to values as low as 10-12‰. Values of $\delta^{13}C$, however, all fall within the range expected for marbles derived from marine carbonates (-2 to +2‰) (Keith and Weber, 1964). We interpret the dramatic change of carbonate $\delta^{18}O$ to be the result of exchange with the metasomatic fluids that formed the talc. Furthermore, these fluids must

have had low $\delta^{18}O$ values. We believe the near constancy of $\delta^{13}C$ indicates that the metasomatic fluids were rich in oxygen and poor in carbon, namely water-rich fluids that contained very little CO_2. A water-rich fluid in excess (high fluid to rock ratio) has the capacity to change $\delta^{18}O$ of the carbonate because of the large quantity of oxygen in the fluid relative to the quantity of oxygen in the rock. If the fluid has only a small amount of CO_2, even with a high fluid to rock ratio, the quantity of carbon in a marble may greatly exceed the quantity of carbon available in the fluid. If the fluid did contain a large amount of CO_2, the absence of significant change in $\delta^{13}C$ would require the unlikely case of an altering fluid already in isotopic equilibrium with the original marble. A water-rich fluid is also consistent with the presence of the mineral assemblage talc+calcite at low temperature, as noted above.

Although $\delta^{13}C$ is very similar for all samples in Figure 13, samples with lower values of $\delta^{18}O$ also tend to have slightly lower values of $\delta^{13}C$. This variation is consistent with loss of CO_2 by decarbonation of dolomite or calcite during talc formation. CO_2 is isotopically heavier in both carbon and oxygen than either calcite or dolomite, so decarbonation reactions would reduce both $\delta^{18}O$ and $\delta^{13}C$ in the remaining carbonate (Raleigh distillation). Raleigh distillation can account for only a small part of the change in $\delta^{18}O$, however, because so much oxygen remains in the rock (Valley, 1986).

$\delta^{18}O$ and $\delta^{13}C$ for carbonate samples from the American Chemet Mine are shown in Figure 14. These data show the same trends as those in Figure 13, but there is more scatter and several of the samples are less homogeneous. Most of the samples labeled calcite also contain some dolomite. Although we expected that the marbles that were all dolomite would have seen the most fluid and, therefore, would have the lowest $\delta^{18}O$ values, we have not been able to make this correlation. Interestingly, the cluster of 5 points with the highest $\delta^{18}O$ values are all calcite marble samples collected on strike several hundred meters from the talc body. Perhaps more systematic sampling of marble as a function of distance from the talc mines would reveal further trends.

All of our $\delta^{18}O$ and $\delta^{13}C$ data for carbonate samples from the Ruby Range talc localities are shown in Figure 15 and are tabulated in Table 1. Regional trends are similar to those of the Regal-Keystone Mine (Figure 13), if not as sharply delineated. Isotopically similar, water-rich fluids apparently circulated through marbles at localities across the Ruby Range and lowered carbonate $\delta^{18}O$ values to as low as 8-10‰. Based on the calcite-water and dolomite-water $\delta^{18}O$ fractionation data of Friedman and O'Neil (1977, summarized here as Figure 16), the Ruby Range oxygen data for carbonates place constraints on the temperature and/or isotopic composition of the talc-forming fluids. (1) The talc-forming fluid cannot be undiluted magmatic water ($\delta^{18}O$ =6-14‰) because at the temperatures permitted for the assemblage talc + calcite (<450°C), magmatic water alone could not lower dolomite $\delta^{18}O$ to 9‰. (2) If the talc-forming fluid was seawater ($\delta^{18}O$ =0‰), then oxygen exchange with dolomite must have occurred at temperatures of **at least** 275 (±20)°C. At lower temperatures (larger fractionation factors), reaction with seawater could not have reduced the dolomite $\delta^{18}O$ values to as little as 9‰. This assumes, of course, that Proterozoic seawater was isotopically similar to modern seawater (Muehlenbachs, 1986). (3) If the talc-forming fluid was like modern meteoric water ($\delta^{18}O$ = -20 to 0‰), then the minimum temperature of talc formation is less restricted and could be substantially lower. However, for reasonable temperatures (100 to 300°C) any meteoric fluids involved must have had $\delta^{18}O$ values greater than -10‰, which is heavy for modern unreacted meteoric fluids, unless isotopic equilibrium between carbonate and

fluid is not approached.

The oxygen isotopic composition of the carbonates does not place tight constraints on the quantity of water necessary to produce the talc deposits. Because there is almost as much oxygen per m^3 of hot water as there is per m^3 of rock, a volumetric water/rock value as low as 2 to 4 could produce the lowering of $\delta^{18}O$ observed for most samples from typical high grade marble values.

Talc

Oxygen isotope data were also collected for several samples of talc (Table 2). Observed $\delta^{18}O$ values are in the range of 4.7-8.8‰. Most of these values are unusually low for silicate minerals in a high grade marble (Valley, 1986) and we believe they reflect equilibration with talc-forming fluids at low temperatures. To our knowledge, there are no experimental calibrations of talc-water ^{18}O fractionation. However, published estimates of $\Delta^{18}O$ (talc-water) based on two different models agree quite well, as shown in Figure 17 (Savin and Lee, 1988; Zheng, 1993). If the models are correct, then the talc $\delta^{18}O$ data place important constraints on the temperature and/or composition of the fluid that are similar to constraints from the carbonate $\delta^{18}O$ data. (1) If the talc-forming fluid was seawater ($\delta^{18}O$ =0‰), then the alteration must have occurred at temperatures of **at least** 275 (±20)°C. Reaction at lower temperatures (larger fractionation factors) could not have produced talc of 4.7‰. (2) If meteoric water was involved, it would have been rather heavy ($\delta^{18}O$ > -10‰), if isotopic equilibrium between talc and fluid was approached. Both of these "constraints" must be viewed with caution because the $\Delta^{18}O$ (talc-water) curves are theoretical. However, these results are quite similar to those for the carbonate data.

The $\Delta^{18}O$ (talc-water) models of Savin and Lee (1988) and Zheng (1993) can be combined with the $\Delta^{18}O$ (calcite-water) and $\Delta^{18}O$ (dolomite-water) calibrations of Friedman and O'Neil (1977) to define $\Delta^{18}O$ (talc-calcite) and $\Delta^{18}O$ (talc-dolomite) geothermometers. Two of the talc samples analyzed (ACL-RK-001a and JBB-AC-30) also contained dolomite. $\Delta^{18}O$ (talc-dolomite) for these samples are shown in Figure 18 along with the calculated $\Delta^{18}O$ (talc-dolomite) geothermometer. Temperatures suggested by these data are neither consistent nor geologically reasonable. Although the $\Delta^{18}O$ (talc-dolomite) geothermometer is theoretical, we interpret these data as an indication that talc and dolomite were not in isotopic equilibrium. This is consistent with the large range of $\delta^{18}O$ values observed for both talc and carbonate.

Five talc samples analyzed for ^{18}O were also analyzed for D/H. Observed D/H values range from -49.9 to -57.6 ‰ (SMOW, Table 2). We know of no experimental or theoretical hydrogen isotope fractionation factors for ΔD/H (talc-water) with which to interpret these data. Suzuoki and Epstein (1976) published hydrogen isotope fractionation curves for several other OH-bearing minerals in the range of 400-850°C based on experimental data. They conclude that hydrogen isotopic fractionation is a function of temperature and the molar fraction of octahedrally-coordinated cations (Al, Mg, Fe) in the crystal, due to bonding of the OH groups to octahedral sites. If this is true for talc, then a fractionation factor for talc-water might be similar to Suzuoki and Epstein's experimentally derived fractionation factor for muscovite-water because of the structural similarities between muscovite and talc.

Extrapolating the Suzuoki and Epstein (1976) hydrogen geothermometer for muscovite-water from its experimental range (400° to 850°C) to lower temperatures and using it to evaluate the talc D/H data, we find the hydrogen isotope data are consistent with a model of talc formation from seawater (SMOW) at temperatures of 200°-300°C. Because of the uncertainty in the fractionation model, the hydrogen data do not presently provide a strong constraint on the composition of the talc-forming fluid.

Graphite

Carbon isotopic data were collected for graphite from several samples in which the carbonate was analyzed (Table 3). To help interpret these data, the $\Delta^{13}C$ (calcite-graphite) geothermometer of Dunn and Valley (1992) is shown in Figure 19. Also shown is a model $\Delta^{13}C$ (dolomite-graphite) geothermometer calculated by subtracting the Sheppard and Schwartz (1970) equation for $\Delta^{13}C$ (dolomite-calcite) from Dunn and Valley's equation for $\Delta^{13}C$ (calcite-graphite). Observed values of $\Delta^{13}C$ (calcite-graphite) and $\Delta^{13}C$ (dolomite-graphite) appear to record temperatures between 600 and 700°C. Based on evidence already discussed, these temperatures are clearly too high for the talc-forming event. The calculated temperatures are more appropriate for the Archean upper amphibole facies metamorphism, if a bit low, and imply little or no reequilibration of the carbon isotopes among these minerals during talc formation. Graphite is notoriously refractory, so it is perhaps not surprising that values of $\delta^{13}C$ for graphite in marbles completely altered to massive talc rocks are similar to $\delta^{13}C$ values for graphite in unaltered marbles. However, replacement of calcite by dolomite probably would change the carbonate $\delta^{13}C$ values and, therefore, $\Delta^{13}C$ (carbonate-graphite), if the metasomatic fluid were CO_2-rich. We believe the $\delta^{13}C$ data provide additional evidence that the fluid was carbon-poor (water-rich).

Discussion

Seawater is known to be an effective agent for Mg-metasomatism in the formation of dolomite (e.g. Whitaker et al., 1994), especially at high temperatures (Morrow and Abercrombie, 1994; Usdowski, 1994), and in the hydrothermal alteration of oceanic crust (Seyfried and Bischoff, 1979). Other rocks in the Ruby Range are not especially Mg-rich, so it is unlikely that meteoric water could be sufficiently enriched in Mg by nearby rocks to convert a calcite marble to talc. Seawater may have been available in the region at the time of talc formation (1360 Ma) due to the nearby faulting and continental flooding associated with the opening of the Belt Basin (McMannis, 1963). Anderson et al. (1990) suggested seawater as a possible source for the fluid that produced the Ruby Range talc deposits and proposed Belt Basin rifting as a mechanism to supply the seawater. We believe our isotopic data offer strong evidence in favor of seawater as the talc-forming fluid and support the Anderson et al. (1990) model connecting talc formation to the Belt Basin opening.

Talc is apparently forming today in the Gulf of California and elsewhere by direct precipitation from marine hydrothermal fluids. Londsdale et al. (1980) describe ledges of talc that they observed and sampled on a submersible dive near a spreading axis in the Guaymas Basin. Their isotopic data for talc ($\delta^{18}O$ = 5.3(3)‰, D/H = -38.0‰ SMOW) and their calculated temperature of formation (280°C) are remarkably close to the isotopic data we observed and formation temperature we calculated for talc in Montana. Costa et al. (1980) describe "bedded sedimentary talc" adjacent

to ancient sea-floor hydrothermal vents in Archean greenstone belts in Quebec. The measured oxygen isotopic values for the bedded talc ($\delta^{18}O$ = 5.2 to 6.6‰) also are similar to the Montana values. That modern and Archean marine hydrothermal fluids can precipitate talc with oxygen and hydrogen isotopic values that match the Ruby Range talc clearly supports the idea that seawater is a plausible metasomatic fluid for making talc in the Ruby Range.

Based on isotopic data, deep (>10km) circulation of seawater has been suggested by Wickham and Taylor (1987) as coinciding with a Hercynian rifting event in the Pyrenees. Their oxygen and carbon isotope data on carbonates (their Figure 9) show trends similar to those we observed for the Ruby Range (Figure 15). Our Ar data show that the Ruby Range talc formed at the time (1360 Ma) that the Belt Basin was developing due to continental rifting. Perhaps circulation of seawater along faults in continental crust is common in rift environments. Active faulting might facilitate fluid circulation by "seismic pumping" (Sibson et al., 1975). Elevated heat flow in a rift environment may have provided the elevated temperatures needed to produce talc at depths attainable by circulating seawater.

Summary

A plausible model for talc formation in SW Montana begins with upper amphibolite facies metamorphism of an Archean rock package that contains limestones. Geochronological data require at least two regional metamorphic events: one at 2.7-3.1 Ga and another at 1.7-1.8 Ga. We know that at least one metamorphic event was at upper amphibolite facies conditions (650°to 750°C, 0.8-1.0 GPa) and that the 1.7-1.8 Ga event was at temperatures in excess of 525°C. At about 1.4 Ga, SW Montana underwent extension that produced faults with a NW trend (in today's coordinate system) and was intruded by a swarm of basalt dikes, also with a NW trend. Extension and resulting crustal thinning allowed the ocean to transgress onto the continental margin. Seawater penetrated the crust along some of the normal faults to depths (5-10 km?) at which the temperature was between 250° and 350°C. Heating of the seawater by the anomalous crustal geotherm caused the water to rise and led to the development of a large-scale circulation of seawater. Circulation of the fluid was influenced by faults, folds, and contacts between marble and gneiss. Where the heated seawater came into contact with calcite marble, the marble was first dolomitized and then converted to talc. Where the heated seawater came into contact with quartzofeldspathic gneiss, feldspar in the gneiss was first altered to fine-grained muscovite and then converted to chlorite. Chemical effects of the fluid were principally to add Mg, Si, H, ^{16}O and to remove Ca, Al, C, D, ^{18}O. Sufficient fluid passed certain areas to completely overwhelm the buffering capacity of the minerals in the rocks, making this a fluid-dominated environment.

Acknowledgments

The field and lab work were part of an undergraduate summer research project sponsored by the Keck Geology Consortium (Amherst College, Beloit College, Carleton College, College of Wooster, Colorado College, Franklin and Marshall College, Pomona College, Smith College, Trinity University, Washington and Lee University, Whitman College, Williams College) with funding from the W.M. Keck Foundation. This report is an outgrowth of the resulting senior theses and could not have been completed without the support of the Keck Foundation and the twelve colleges of the consortium. We thank John Childs, Dave Mogk, Pete Dahl, Mae Gustin,

and Dave Van Alstine for sharing unpublished data and maps. We thank Page Chamberlain and Libby Stern for making the oxygen isotope laboratory at Dartmouth available and friendly. We thank Steve Dunn for help with the graphite separation. We thank Dan Lux and his assistants at the University of Maine for collecting the $^{40}Ar/^{39}Ar$ data. We thank Art Christensen and Buster Brown for giving advice in the field and access to talc occurrences on their properties. We thank Eric Hovestol and Bob Piniazkiewicz for advice and information about the Yellowstone Talc deposit. Initial work on the talc deposits by John Brady was funded by the U.S Geological Survey with the guidance and support of Byron R. Berger. The manuscript was improved by the unusually careful and thoughtful reviews of John Goodge and Dave Mogk.

References cited

Anderson, D.L. (1987) Timing and mechanism of formation of selected talc deposits in the Ruby Range, southwestern Montana. 90 p., unpublished M.S. thesis, Montana State University.

Anderson, D.L., Mogk, D.W., and Childs, J.F. (1990) Petrogenesis and timing of talc formation in the Ruby Range, southwestern Montana. Economic Geology, 85, 585-600.

Berg, R.B. (1979) Talc and chlorite deposits in Montana. 66 p., Montana Bureau of Mines and Geology Memoir 45.

Berman, R. (1988) Internally-consistent thermodynamic data for minerals in the system Na_2O-K_2O-CaO-MgO-FeO-Fe_2O_3-Al_2O_3-SiO_2-TiO_2-H_2O-CO_2. Journal of Petrology, 29, 445-522.

Bigeleisen, J., Perlman, M.L., and Prosser, H.C. (1952) Conversion of hygenic materials to hydrogen for isotopic analysis. Analytical Chemistry, 24, 1356-1357.

Brady, J.B., Burger, H.R., Cheney, J.T., King, J.T., Tierney, K.A., Peck, W.H., Poulsen, C.J., Cady, P., Lowell, J, Sincock, M.J., Archuleta, L.L., Fisher, R., and Jacob, L. (1994) Geochemical and $^{40}Ar/^{39}Ar$ evidence for terrain assembly in the Archean of southwestern Montana. Geological Society of America Abstracts with Programs, 26, A232-A233.

Clayton, R.N., and Mayeda, T.K. (1963) The use of bromine penta-fluoride in the extraction of oxygen from oxides and silicates for isotopic analysis. Geochimica et Cosmochimica Acta, 27, 43-52.

Costa, U.R., Fyfe, W.S., Kerrich, R., and Nesbitt, H.W. (1980) Archean hydrothermal talc evidence for high ocean temperatures. Chemical Geology, 30, 341-349.

Criss, R.E., (1995) Stable isotope distribution. variations from temperature, organic and water-rock interactions. In T.J. Ahrens, ed., Global Earth Physics: A Handbook of Physical Constants, 1, 292-307, American Geophysical Union, Washington, D.C.

Dahl, P. (1979) Comparative geothermometry based on major element and oxygen isotope distributions in Precambrian metamorphic rocks from southwestern Montana. American Mineralogist, 64, 1280-1293.

Dahl, P. (1980) The thermal-compositional dependence of Fe^{2+}-Mg distributions between coexisting garnet and pyroxene: applications to geothermometry. American Mineralogist, 65, 854-866.

Desmarais, N.R. (1981) Metamorphosed Precambrian ultramafic rocks in the Ruby Range, Montana. Precambrian Research, 16, 67-101.

Dunn, S.R., and Valley, J.W. (1992) Calcite-graphite isotope thermometry: a test for polymetamorphism in marble, Tudor gabbro aureole, Ontario, Canada. Journal of Metamorphic Geology, 10, 487-501.

Friedman, I., and O'Neil, J.R. (1977) Compilation of stable isotope fractionation factors of geochemical interest. In M. Fleischer, editor, Data of Geochemistry, 6th Edition, U.S. Geological Survey Professional Paper 440-KK.

Garihan, J.M. (1973) Geology and talc deposits of the central Ruby Range, Madison Country, Montana. 209 p., unpublished Ph.D. dissertation, Pennsylvania State University.

Garihan, J.M. (1976) Geologic road log from Dillon to Alder, covering the Precambrian geology of the central Ruby Range, Madison County, southwestern Montana. Montana Bureau of Mines and Geology Special Publication 73, 15-26.

Giletti, B. (1966) Isotopic ages from southwestern Montana. Journal of Geophysical Research, 71, 4029-4036.

Hodges, K.V., Hames, W.E., and Bowring, S.A. (1994) $^{40}Ar/^{39}Ar$ age gradients in micas from a high-temperature low-pressure metamorphic terrain -- evidence for very slow cooling and implications for the interpretation of age spectra. Geology, 22, 55-58.

Holdaway, M.J., Dutrow, B.L., Borthwick, J., Shore, P., Harmon, R.S., and Hinton, R.W. (1986) H content of staurolite as determined by H extraction line and ion microprobe. American Mineralogist, 71, 1135-1141.

James, H.L. (1990) Precambrian geology and bedded iron deposits of the southwestern Ruby Range, Montana. 39 p., U.S. Geological Survey Professional Paper 1495.

James, H.L. and Hedge, C.E. (1980) Age of the basement rocks of southwest Montana. Geological Society of America Bulletin, 91, 11-15.

Karasevich, L.P., Garihan, J.M., Dahl, P.S., and Okuma, A.F. (1981) Summary of Precambrian metamorphic and structural history, Ruby Range, southwest Montana. Geological Society of Montana 1981 Field Conference Guidebook, 225-237.

Keith, M.L., and Weber, J.N. (1964) Carbon and oxygen isotopic composition of selected limestones and fossils. Geochimica et Cosmochimica Acta, 28, 1787-1816.

Korzhinskii, D.S. (1970) Theory of metasomatic zoning. 162 p., Oxford University Press.

Kovaric, D.N., Brady, J.B., Cheney, J.T., Grove, M. , Jacob, L.J., King, J.T. (1996) $^{40}Ar/^{39}Ar$ evidence for reheating events affecting basement rocks in the Tobacco Root, Ruby, and Highland Mountains, SW Montana. Geological Society of America Abstracts with Programs, 28, A-493.

Krogh, T.E., and Hess, D.F. (1997) Wyoming province 3300+ Ma gneiss with 2400 Ma metamorphism, northwestern Tobacco Root Mountains, Madison Co., Montana. Geological Society of America Abstracts with Programs, 29, A-408.

Larson, A.C. (1991) Talc formation in the Regal-Keystone mine of the Ruby Range, Dillon, Montana. 57 p., unpublished B.A. thesis, Smith College.

Lonsdale, P.F., Bischoff, J.L., Burns, V.M., Kastner, M., and Sweeney, R.E. (1980) A high-temperature hydrothermal deposit on the seabed at a Gulf of California spreading center. Earth and Planetary Science Letters, 49, 8-20.

Lux, D.R., Gibson, D., and Hamilton, P.J. (1989) Geochronology of the Songo pluton, western Maine. In Studies in Maine Geology, 4, 101-114, Maine Geological Survey.

McCrea, J.M. (1950) On the isotopic chemistry of carbonates and a paleotemperature scale. Journal of Chemical Physics, 18, 849-857.

McDougall, I., and Harrison, T.M. (1988) Geochronology and thermochronology by the $^{40}Ar/^{39}Ar$ method. 212 p., Oxford University Press, New York.

McMannis, W.J. (1963) LaHood Formation -- a coarse facies of the Belt Series in southwestern Montana. Geological Society of America Bulletin, 74, 407-436.

Morrow, D.W., and Abercrombie, H.J. (1994) Rates of dolomitization: the influence of dissolved sulphate. In Purser, B., Tucker, M., and Zenger, D., editors, Dolomites, 377-386, International Association of Sedimentologists, Special Publication 21.

Mueller, P.A., and Cordua, W.S. (1976) Rb-Sr whole rock age of gneisses from the Horse Creek area, Tobacco Root Mountains, Montana. Isochron West, 16, 33-36.

Mueller, P.A., Wooden, J., Heatherington, A., and Nutman, A. (1997) Distribution of Proterozoic crust along the NW margin of cratonic North America: evidence from U-Pb zircon ages and isotopic systematics in young granitoids. Geological Society of America Abstracts with Programs 29, A-70.

Muehlenbachs, K. (1986) Alteration of the oceanic crust and the ^{18}O history of seawater. In Valley, J.W., Taylor, H.P., Jr., and O'Neil, J.R., editors, Stable Isotopes in High Temperature Geological Processes, Reviews in Mineralogy Volume 16, 425-444, Mineralogical Society of America, Washington, D.C.

Okuma, A.F. (1971) Structure of the southwestern Ruby Range near Dillon, Montana. 122 p., unpublished Ph.D. dissertation, Pennsylvania State University.

Olson, R.H. (1976) The geology of Montana talc deposits. Montana Bureau of Mines and Geology Special Publication 74, 99-143.

O'Neil, J.R. (1986) Terminology and standards. In Valley, J.W., Taylor, H.P., Jr., and O'Neil, J.R., editors, Stable Isotopes in High Temperature Geological Processes, Reviews in Mineralogy Volume 16, 561-570, Mineralogical Society of America, Washington, D.C.

O'Neill, J.M., Duncan, M.S., and Zartman, R.E. (1988) An early Proterozoic gneiss dome in the Highland Mountains, southwestern Montana. Montana Bureau of Mines and Geology Special Publication 96, 81-88.

Savin, S.M., and Lee, W. (1988) Isotopic studies of phyllosilicates. In Bailey, S.W., editor, Hydrous Phyllosilicates, Reviews in Mineralogy Volume 19, 189-223, Mineralogical Society of America, Washington, D.C.

Schmidt, C.J. and Garihan, J.M. (1986) Middle Proterozoic and Laramide tectonic activity along the southern margin of the Belt basin. Montana Bureau of Mines and Geology Special Publication 94, 217-235.

Seyfried, W.E., and Bischoff, J.L. (1979) Low temperature basalt alteration by seawater: an experimental study at 70°C and 150°C. Geochimica et Cosmochimica Acta, 43, 1937-1947.

Sheppard, S.M.F., and Schwartz, H.P. (1970) Fractionation of carbon and oxygen isotopes and magnesium between coexisting metamorphic calcite and dolomite. Contributions to Mineralogy and Petrology, 20, 306-356.

Sibson, R.H., Moore, J.M., and Rankin, A.H. (1975) Seismic pumping -- a hydrothermal fluid transport mechanism. Journal of the Geological Society of London, 131, 653-659.

Stern, L.A., Chamberlain, C.P., Barnett, D.E., and Ferry, J.M. (1992) Stable isotope evidence for regional-scale fluid migration in a Barrovian metamorphic terrane, Vermont, USA. Contributions to Mineralogy and Petrology, 112, 475-489.

Stettner, G. (1959) Die Lagerstätte des Specksteins von Göpfersgruen-Thiersheim im Fichtelgebirge. Geologica Bavarica, 42, 72 p.

Suzuoki, T., and Epstein, S. (1976) Hydrogen isotope fractionation between OH-bearing minerals and water. Geochimica et Cosmochimica Acta, 40, 1229-1240.

Tysdal, R.G. (1976) Geologic map of northern part of Ruby Range, Madison County, Montana. U.G. Geological Survey Miscellaneous Investigations Series, Map I-951.

Usdowski, E. (1994) Synthesis of dolomite and geochemical implications. In Purser, B., Tucker, M., and Zenger, D., editors, Dolomites, 245-360, International Association of Sedimentologists, Special Publication 21.

Valley, J.W. (1986) Stable isotope geochemistry of metamorphic rocks. In Valley, J.W., Taylor, H.P., Jr., and O'Neil, J.R., editors, Stable Isotopes in High Temperature Geological Processes, Reviews in Mineralogy Volume 16, 445-489, Mineralogical Society of America, Washington, D.C.

Vasquez, A.M. (1991) A comparative analysis of talc deposits in the Ruby Range, southwest Montana. 93 p., unpublished B.A. thesis, Amherst College.

Vitaliano, C.J., Burger, H.R., Cordua, W.S., Hanley, T.B., Hess, D.F., Root, F.K., and Tolen, J.R. (1979) Geologic map of the southern Tobacco Root Mountains, Madison County, Montana. Geological Society of America Map and Chart Series, MC-31.

Walther, J.V., and Orville, P.M. (1983) The extraction-quench technique for determination of the thermodynamic properties of solute complexes: application to quartz solubility in fluid mixtures. American Mineralogist, 68, 731-741.

Whitaker, F.F., Smart, P.L., Vahrenkamp, V.C., Nicholson, H., and Wogelius, R.A. (1994) Dolomitization by near-normal seawater? Field evidence from the Bahamas. In Purser, B., Tucker, M., and Zenger, D., editors, Dolomites, 111-132, International Association of Sedimentologists, Special Publication 21.

Wickham, S.M., and Taylor, H.P, Jr. (1987) Stable isotope constraints on the origin and depth of penetration of hydrothermal fluids associated with Hercynian regional metamorphism and crystal anatexis in the Pyrenees. Contributions to Mineralogy and Petrology, 95, 255-268.

Wooden, J.L., Mueller, P.A., and Mogk, D.W. (1988) A review of the geochemistry and geochronology of the Archean rocks of the northern part of the Wyoming Province. In W.G. Ernst, ed., Metamorphism and Crustal Evolution of the Western United States, 383-410, Prentice-Hall, Englewood Cliffs, NJ.

Wooden, J.L., Vitaliano, C.J., Koehler, S.W., and Ragland, P.C. (1978) The late Precambrian mafic dikes of the southern Tobacco Root Mountains, Montana. Geochemistry, Rb-Sr geochronology, and relationship to Belt tectonics. Canadian Journal of Earth Science, 15, 467-479.

Zheng, Y.-F. (1993) Calculation of oxygen isotope fractionation in hydroxl-bearing silicates. Earth and Planetary Science Letters, 120, 247-263.

Table 1. Carbonate isotope data.

Sample		$\delta^{13}C$ (‰) PDB	$\delta^{13}C$ (‰) Average (±1σ) PDB	$\delta^{18}O$ (‰) SMOW	$\delta^{18}O$ (‰) Average (±1σ) SMOW
ACL-RK-001Aa1	Dol	-0.50	-0.4(1)	20.00	19.8(2)
ACL-RK-001Aa2	Dol	-0.38		19.90	
ACL-RK-001Aa	Dol	-0.36		19.58	
ACL-RK-002A	Dol	-0.65	-0.7(1)	19.40	19.3(1)
ACL-RK-002B	Dol	-0.71		19.20	
ACL-RK-003A	Dol	-0.38	-0.4(1)	19.50	19.4(1)
ACL-RK-003B	Dol	-0.39		19.30	
ACL-RK-007B1	Dol	-0.79	-0.9(1)	17.10	17.1(1)
ACL-RK-007B2	Dol	-0.90		17.10	
ACL-RK-012F1	Dol	-1.63	-1.7(1)	11.00	11.1(1)
ACL-RK-012F2	Dol	-1.66		11.10	
ACL-RK-014D1	Dol	-1.74	-1.8(1)	10.20	10.3(1)
ACL-RK-014D2	Dol	-1.86		10.40	
ACL-RK-015A1	Dol	-0.73	-0.8(1)	14.80	15.0(3)
ACL-RK-015A2	Dol	-0.79		15.20	
ACL-RK-18A1	Dol	-0.86	-0.9(1)	18.40	18.4(1)
ACL-RK-18A2	Dol	-0.89		18.30	
ACL-RK-18B1	Cal	-1.61	-1.6(1)	15.20	15.2(1)
ACL-RK-18B2	Cal	-1.59		15.20	
ACL-RK-18C1	Cal	-1.44	-1.5(1)	14.90	14.9(1)
ACL-RK-18C2	Cal	-1.49		14.90	
ACL-RK-20A1	Cal	-1.70	-1.7(1)	14.20	14.2(1)
ACL-RK-20A2	Cal	-1.69		14.20	
ACL-RK-22B1	Dol	-1.80	-1.8(1)	10.30	10.5(2)
ACL-RK-22B2	Dol	-1.79		10.60	
ACL-RK-026A	Dol	-1.25	-1.3(1)	10.60	10.6(1)
ACL-RK-026B	Dol	-1.29		10.50	
ACL-RK-028A	Cal	-0.61	-0.6(1)	22.90	22.8(2)
ACL-RK-028B	Cal	-0.66		22.60	

Sample		$\delta^{13}C$ (‰) PDB	$\delta^{13}C$ (‰) Average (±1σ) PDB	$\delta^{18}O$ (‰) SMOW	$\delta^{18}O$ (‰) Average (±1σ) SMOW
ACL-RK-029A	Cal	-1.71	-1.7(1)	17.70	17.9(2)
ACL-RK-029B	Cal	-1.69		18.00	
ACL-RK-31D1	Dol	-0.86	-1.0(2)	12.10	12.1(1)
ACL-RK-31D2	Dol	-1.19		12.10	
ACL-RK-31F1	Dol	-1.25	-1.3(1)	17.50	17.5(1)
ACL-RK-31F2	Dol	-1.31		17.40	
ACL-RK-33C1	Dol	-1.03	-1.1(1)	12.50	12.2(5)
ACL-RK-33C2	Dol	-1.09		11.80	
ACL-RK-034A	Dol	-0.21	-0.3(1)	21.10	21.1(1)
ACL-RK-034B	Dol	-0.39		21.10	
ACL-RK-036A1	Dol	0.86	1.0(3)	21.70	22.2(6)
ACL-RK-036A2	Dol	1.21		22.60	
ACL-RK-037B1	Dol	0.35	0.3(1)	23.10	23.2(1)
ACL-RK-037B2	Dol	0.33		23.20	
AMV-RK-4A	Cal	-0.96	-0.9(1)	19.37	19.5(2)
AMV-RK-4B	Cal	-0.88		19.58	
AMV-RK-6A	Dol	-2.06	-1.6(4)	11.81	10.9(8)
AMV-RK-6B	Dol	-1.29		10.30	
AMV-RK-6C	Dol	-1.40		10.60	
AMV-RK-10A	Cal	-2.57	-2.7(1)	10.91	10.9(1)
AMV-RK-10B	Cal	-2.74		10.94	
AMV-RK-12A1	Dol	-0.40	-0.4(1)	19.62	19.7(1)
AMV-RK-12A2	Dol	-0.34		19.72	
AMV-AC-1A	Cal	-2.33	-2.4(1)	8.37	8.3(1)
AMV-AC-1B	Cal	-2.49		8.29	
AMV-AC-10A	Cal	-1.56	-1.5(1)	15.37	15.1(5)
AMV-AC-10B	Cal	-1.51		14.72	
AMV-AC-22A	Dol	-1.56	-1.4(4)	9.50	10.1(9)
AMV-AC-22B	Dol	-0.99		9.65	
AMV-AC-22C	Dol	-1.64		11.18	

Sample		$\delta^{13}C$ (‰) PDB	$\delta^{13}C$ (‰) Average (±1σ) PDB	$\delta^{18}O$ (‰) SMOW	$\delta^{18}O$ (‰) Average (±1σ) SMOW
AMV-AC-31CA	Cal	-4.80	-5.0(3)	16.85	18.1(1.8)
AMV-AC-31CB	Cal	-5.22		19.39	
AMV-AC-32A	Dol	-1.38	-1.3(2)	9.76	9.7(1)
AMV-AC-32B	Dol	-1.13		9.57	
AMV-AC-38A	Dol	-1.62	-1.8(2)	8.87	9.3(7)
AMV-AC-38B	Dol	-1.91		9.80	
AMV-AC-41A	Dol	-1.28	-1.2(1)	9.24	9.5(3)
AMV-AC-41B	Dol	-1.17		9.65	
AMV-AC-43A	Dol	-3.93	-3.3(9)	15.41	16.6(1.6)
AMV-AC-43B	Dol	-2.57		17.68	
JTC-AC-1B1	Cal	-2.16	-1.9(4)	22.55	22.7(1)
JTC-AC-1B2	Cal	-1.57		22.76	
JTC-AC-1D1	Cal	-0.34	-0.3(1)	22.35	22.4(1)
JTC-AC-1D2	Cal	-0.34		22.38	
JTC-AC-1E1	Cal	-0.84	-0.8(1)	20.00	20.1(2)
JTC-AC-1E2	Cal	-0.81		20.23	
JTC-AC-2A1	Cal	-1.01	-1.0(1)	22.53	22.5(1)
JTC-AC-2A2	Cal	-1.06		22.50	
JTC-AC-3A		-1.67	-1.7(1)	11.70	11.6(2)
JTC-AC-3B		-1.76		11.40	
JBB-AC-25A	Cal	-0.65	0.0(9)	13.40	13.1(4)
JBB-AC-25B	Cal	0.72		12.80	
JBB-AC-27A	Dol	-0.38	-0.4(1)	22.70	22.6(1)
JBB-AC-27B	Dol	-0.47		22.50	
JBB-AC-30B	Dol	-1.01	-1.0(1)	9.82	9.8(1)
JBB-AC-30A	Dol	-1.01		9.82	
JBB-AC-37A	Dol	-1.02	-1.0(1)	9.48	9.5(1)
JBB-AC-37B	Dol	-1.05		9.57	
JBB-AC-41A	Dol			9.11	9.2(1)
JBB-AC-41B	Dol			9.29	

Sample		$\delta^{13}C$ (‰) PDB	$\delta^{13}C$ (‰) Average (±1σ) PDB	$\delta^{18}O$ (‰) SMOW	$\delta^{18}O$ (‰) Average (±1σ) SMOW
JBB-AC-62B	Dol	-0.47	-0.5(1)	13.10	13.0(1)
JBB-AC-62A	Dol	-0.50		12.90	
AMV-CC-1A1	Dol	-1.76	-1.5(3)	10.00	9.9(2)
AMV-CC-1A2	Dol	-1.30		9.77	
AMV-CC-1B1	Dol	-0.95	-0.8(2)	17.91	18.6(9)
AMV-CC-1B2	Dol	-0.67		19.19	
AMV-CC-2A2	Dol	-1.45	-1.45	9.61	9.61
AMV-CC-5C1	Dol	-2.62	-2.7(1)	9.94	9.9(1)
AMV-CC-5C2	Dol	-2.74		9.87	
AMV-CC-6A	Cal	-0.93	-0.9(1)	13.62	14.6(1.4)
AMV-CC-6B	Cal	-0.93		15.56	
JBB-CC-2A	Cal	-1.39	-1.28(0.16)	13.40	12.9(7)
JBB-CC-2B	Cal	-1.45		13.50	
JBB-CC-2B	Cal	-1.15		12.11	
JBB-CC-2A	Cal	-1.14		12.47	
AMV-CR-2A	Cal	-2.44	-2.3(2)	17.96	18.3(5)
AMV-CR-2B	Cal	-2.20		18.59	
AMV-CR-3A	Dol	-3.60	-3.3(4)	8.60	9.0(6)
AMV-CR-3B	Dol	-3.07		9.44	
JTC-CR-1A	Cal	1.10	0.8(5)	21.64	21.3(6)
JTC-CR-1B	Cal	0.43		20.86	
JTC-CR-1A1	Dol	-2.33	-2.3(1)	16.10	16.1(1)
JTC-CR-1A2	Dol	-2.29		16.10	
JTC-CR-1B1	Cal	0.23	0.2(1)	18.29	16.4(2.7)
JTC-CR-1B2	Cal	0.08		14.53	
AMV-MP-4A	Cal	-1.03	-1.1(1)	19.35	18.7(9)
AMV-MP-4B	Cal	-1.12		18.12	
AMV-MP-6A	Dol	-0.07	-0.1(1)	19.55	19.8(3)
AMV-MP-6B	Dol	-0.07		19.94	
AMV-MP-12A	Cal	-1.54	-1.4(2)	12.80	12.4(6)
AMV-MP-12B	Cal	-1.24		11.98	

Sample		$\delta^{13}C$ (‰) PDB	$\delta^{13}C$ (‰) Average (±1σ) PDB	$\delta^{18}O$ (‰) SMOW	$\delta^{18}O$ (‰) Average (±1σ) SMOW
AMV-MP-15A1	Dol	0.00	-0.1(1)	12.84	12.6(3)
AMV-MP-15A2	Dol	-0.20		12.40	
AMV-MP-15B1	Dol	-1.12	-1.1(1)	11.28	11.8(7)
AMV-MP-15B2	Dol	-1.12		12.32	
AMV-SD-3A1	Dol	-1.91	-1.5(6)	13.95	14.4(7)
AMV-SD-3A2	Dol	-1.07		14.88	
AMV-SD-4A	Cal	-1.29	-1.2(2)	15.56	14.6(1.3)
AMV-SD-4B	Cal	-1.03		13.69	
AMV-SW-6A	Dol	-2.33	-1.9(6)	14.80	15.3(6)
AMV-SW-6B	Dol	-1.54		15.70	
AMV-SW-11A2	Dol	-3.67	-3.7(1)	9.59	9.7(2)
AMV-SW-11A3	Dol	-3.69		9.83	
AMV-SW-12C	Dol	-1.75	-2.4(9)	12.60	11.8(1.1)
AMV-SW-12D	Dol	-3.10		11.02	
AMV-SW-14A	Dol	-1.26	-1.0(4)	11.83	12.9(1.5)
AMV-SW-14B	Dol	-0.66		13.96	
AMV-SW-17B	Dol	-4.25	-4.1(2)	11.53	11.5(1)
AMV-SW-17C	Dol	-4.12		11.44	
AMV-SW-17D	Dol	-3.91		11.58	
JBB-SW-13B2	Dol	-0.57	-0.6(1)	13.40	13.4(1)
JBB-SW-13B1	Dol	-0.53		13.40	
JBB-SC-8-11A	Cal	-3.79	-4.4(8)	17.80	17.5(4)
JBB-SC-8-11B	Cal	-4.97		17.20	

Abbreviations

Cal Calcite
Dol Dolomite
RK Regal-Keystone Mine
AC American Chemet Mine
CC Cottonwood Creek Prospect (Berg, 1979, Prospect 13)
CR Crescent Ranch Prospect
MP M.P Prospect (Sec. 32)
RP Ruby Peak Prospect
SC Stone Creek Road (Garihan, 1976, Stop 3)
SD Smith-Dillon Mine
SW Sweetwater Mine
SV Sweetwater View Mine

Table 2. Oxygen and hydrogen isotope data for talc.

Sample	Wt.% H_2O	D/H (‰) Talc SMOW	$\delta^{18}O$ (‰) Talc SMOW	$\delta^{18}O$ (‰) Dol SMOW	$\Delta^{18}O$ (‰) Dol-Talc
ACL-RK-001a	4.64	-57.6	8.8(8)	19.8(2)	11(1)
ACL-RK-019A	5.65	-54.9	6.3(2)		
JBB-AC-30	5.30	-53.1	5.0(2)	9.8(2)	4.8(4)
JBB-AC-32	4.94	-49.9	5.6(2)		
JBB-AC-56			4.7(2)		
JBB-TC8-1	4.89	-57.5	5.2(4)		

RK - Regal-Keystone Mine, AC - American Chemet Mine, TC - Treasure Mine

Table 3. Carbon isotope data for graphite and carbonate.

Sample		$\delta^{13}C$ (‰) Graphite PDB	$\delta^{13}C$ (‰) Carbonate PDB	$\Delta^{13}C$ (‰) Carb-Gr
JBB-AC-25	Cal	-5.0	-0.7	4.3
JBB-AC-37	Dol	-4.6	-1.0	3.6
JBB-AC-41	Dol	-5.0	-0.8	4.2
JBB-AC-62	Dol	-1.8	-0.5	1.3
JBB-CC-2	Cal	-5.0	-1.3(6)	3.7
JBB-SC8-7	Cal	-9.7	-4.4(2)	5.3
JBB-SW-9		-4.6(5)	absent	
JBB-TC8-24		-3.8(2)	absent	

AC - American Chemet Mine
CC - Cottonwood Creek Prospect (Berg, 1979, Prospect 13)
SC - Stone Creek Road (Garihan, 1976, Stop 3)
SW - Sweetwater Mine
TC - Treasure Mine

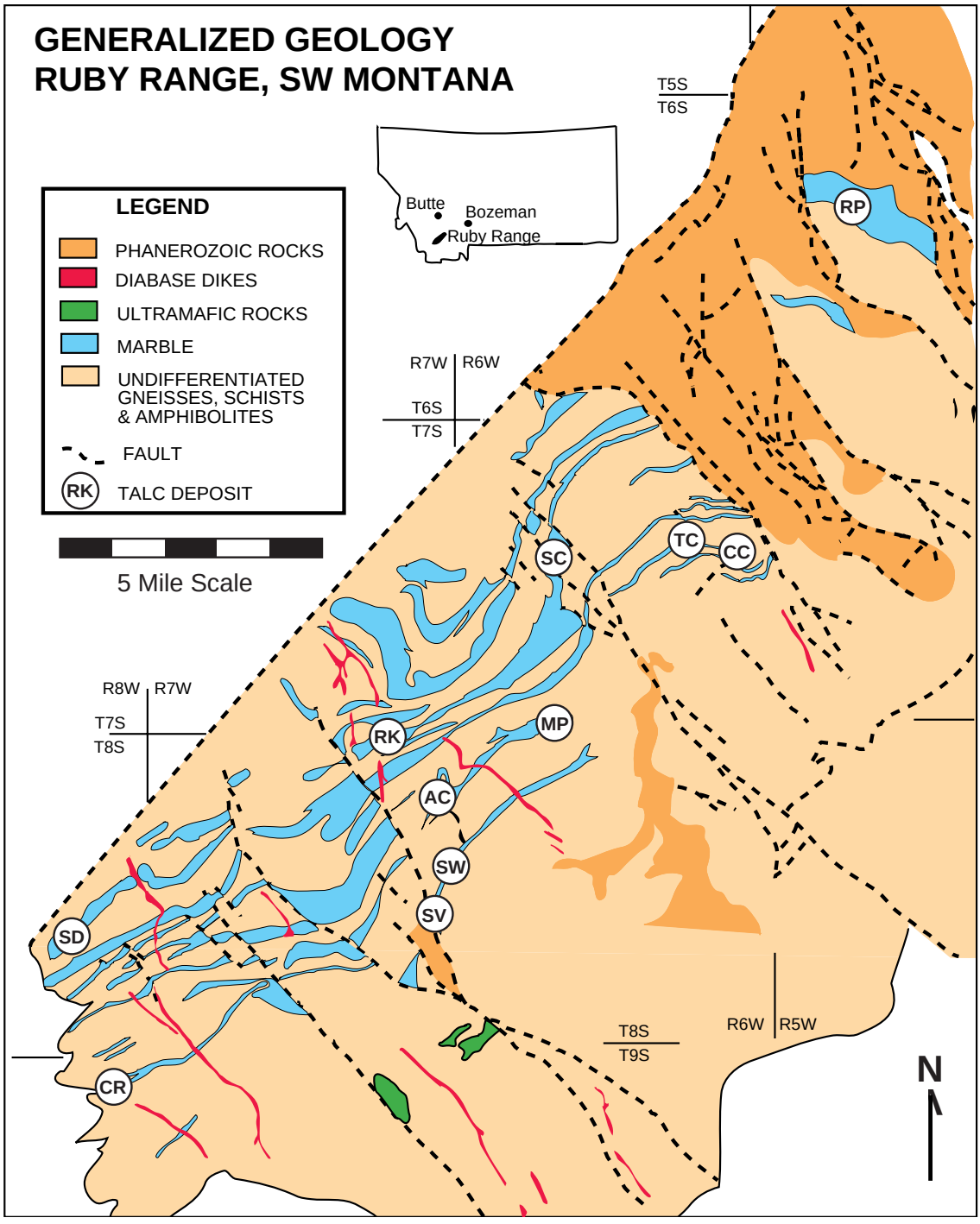

Figure 1. Generalized geologic map of the Ruby Range. Modified from Karasevich et al. (1981). Talc localities are marked with two-letter abbreviations (see Table 1).

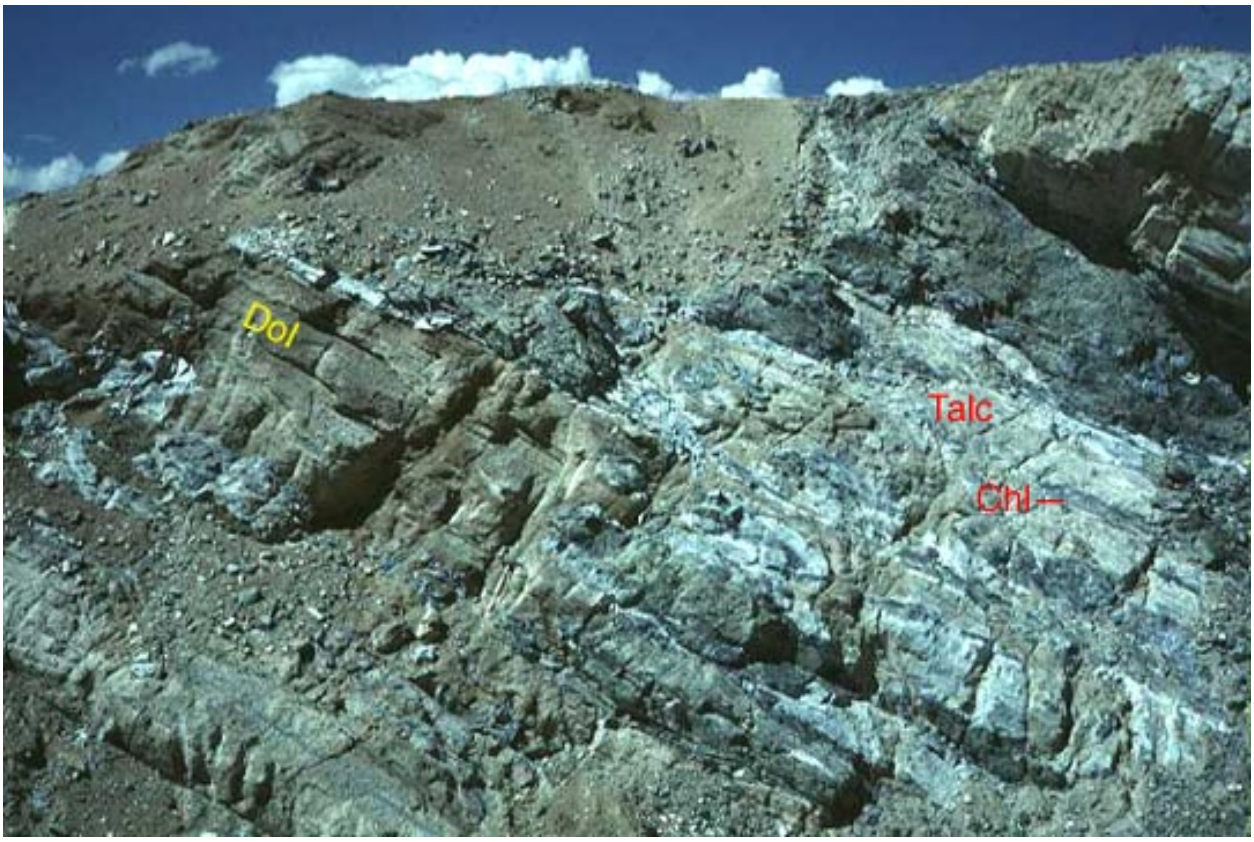

Figure 2. Gray-green talc veins replacing rusty-colored, coarse-grained dolomite (Dol) in the west wall of the Sweetwater Mine. Some talc veins are parallel to bedding, but many are cross-cutting. The darker green sections contain chlorite (Chl). A hammer with a 12-inch-long handle is in the center of the photo for scale.

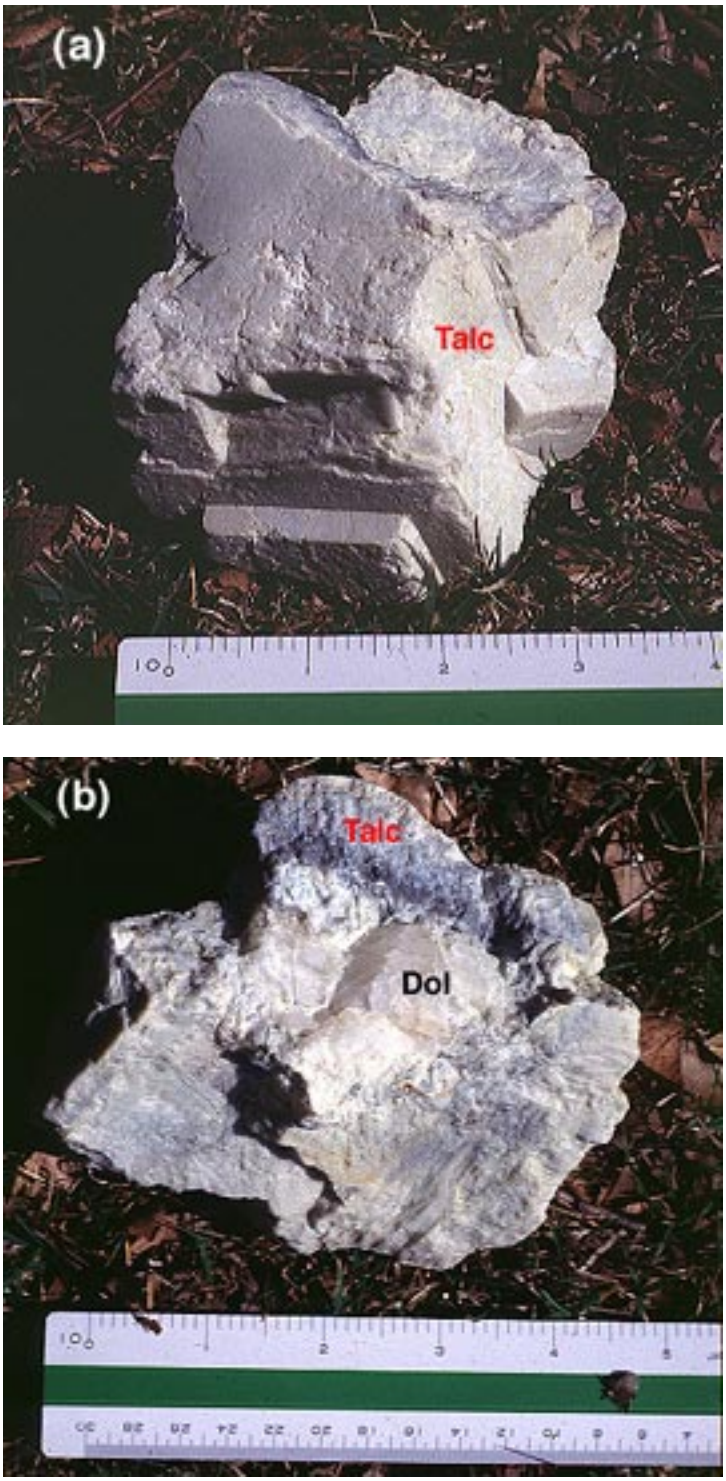

Figure 3. (a) Gray-green, massive talc pseudomorph of a coarse (7-9 cm) dolomite (Dol) crystal collected near the Treasure Mine. Dolomite remains in the core of this crystal as can be seen in Figure 3b. The scale is in inches. (b) Cream-colored dolomite remaining in the core of the gray-green, massive talc pseudomorph shown in (a).

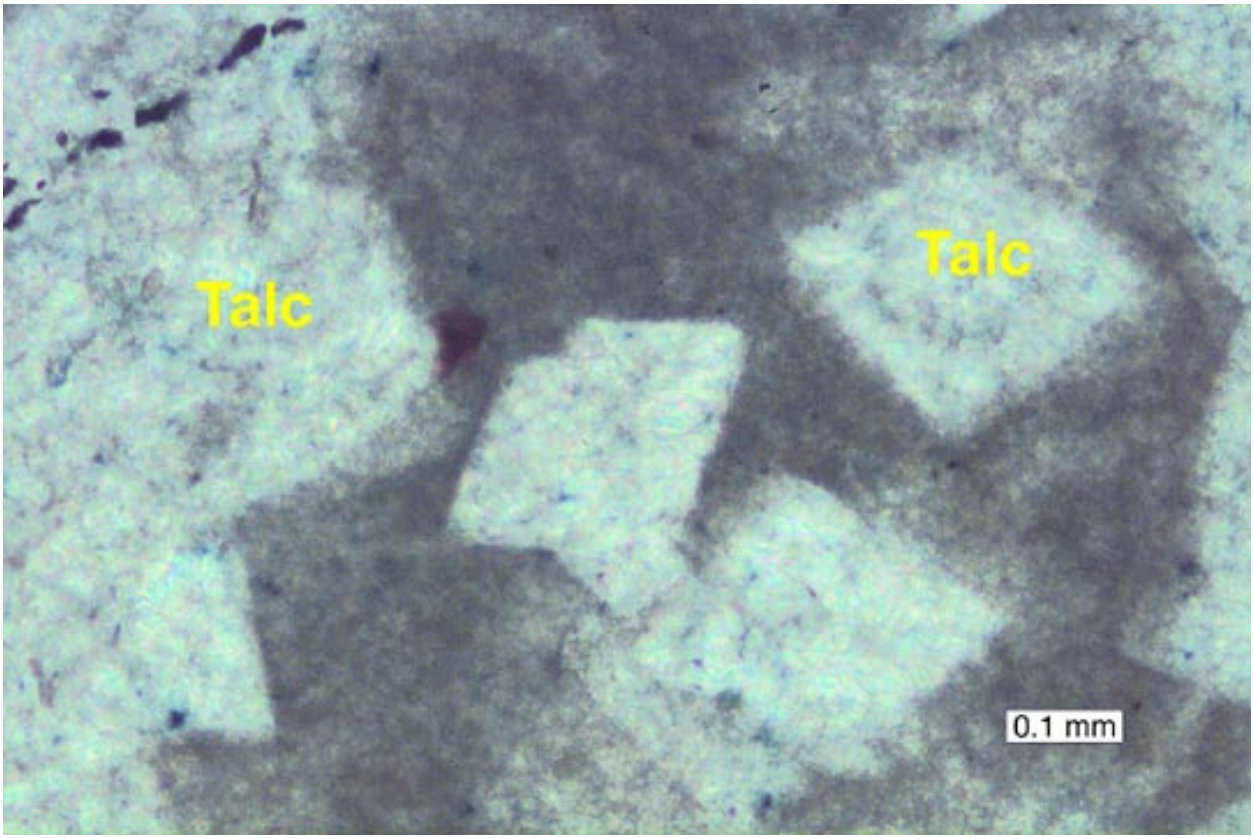

Figure 4. Photomicrograph in crossed polarized light of polycrystalline talc pseudomorphs of dolomite rhombs in a sample from the American Chemet Mine. Nearly everything in the photo is talc. The areas around the rhombs are dark because of a smaller grain size and small quantities of other minerals.

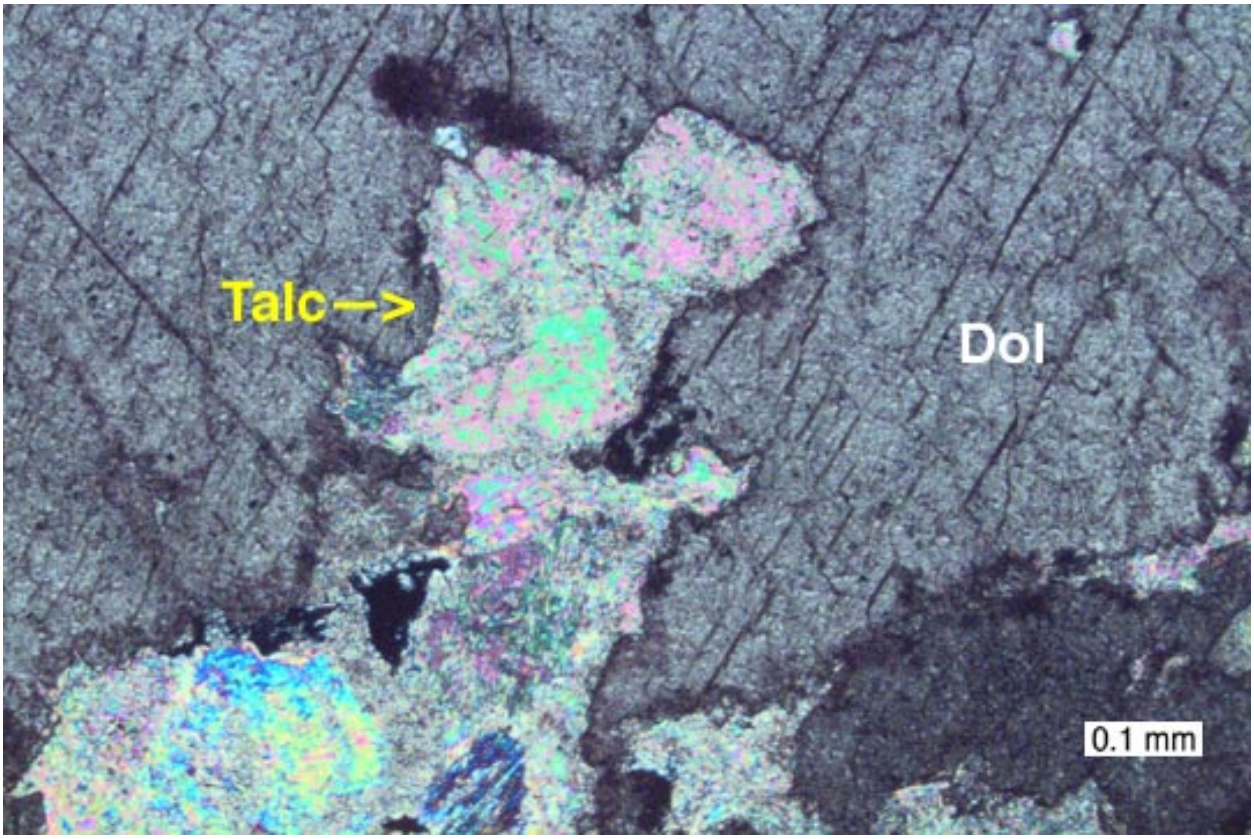

Figure 5. Photomicrograph in crossed polarized light of polycrystalline talc replacing a large dolomite crystal in a sample from the Treasure Mine. Notice that boundaries of talc and dolomite are commonly convex toward the dolomite.

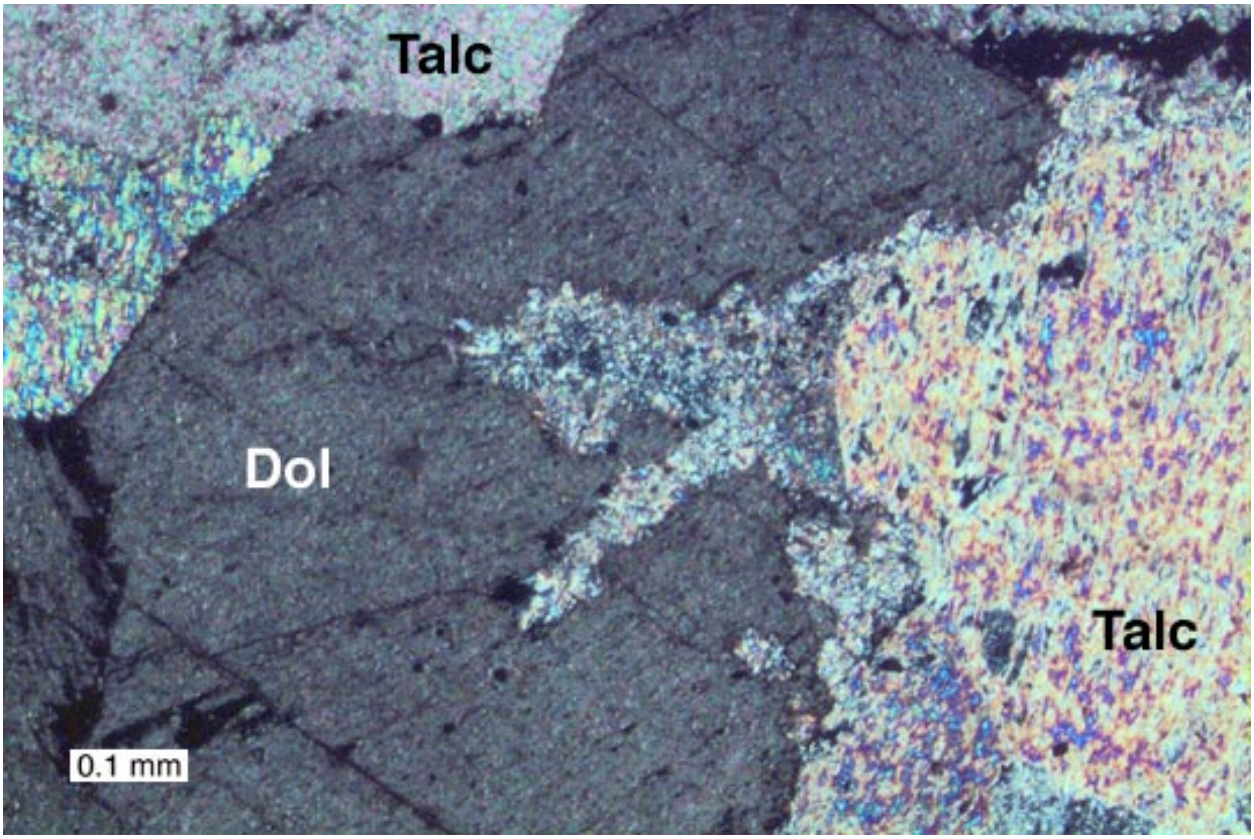

Figure 6. Photomicrograph in crossed polarized light of polycrystalline talc replacing dolomite. The talc appears to be replacing dolomite along fractures as well as along its edges. The talc close to the dolomite tends to be more fine-grained. Coarsening of the talc apparently occurs following its initial growth by the dolomite-fluid reaction. This sample is from the Sweetwater View Mine.

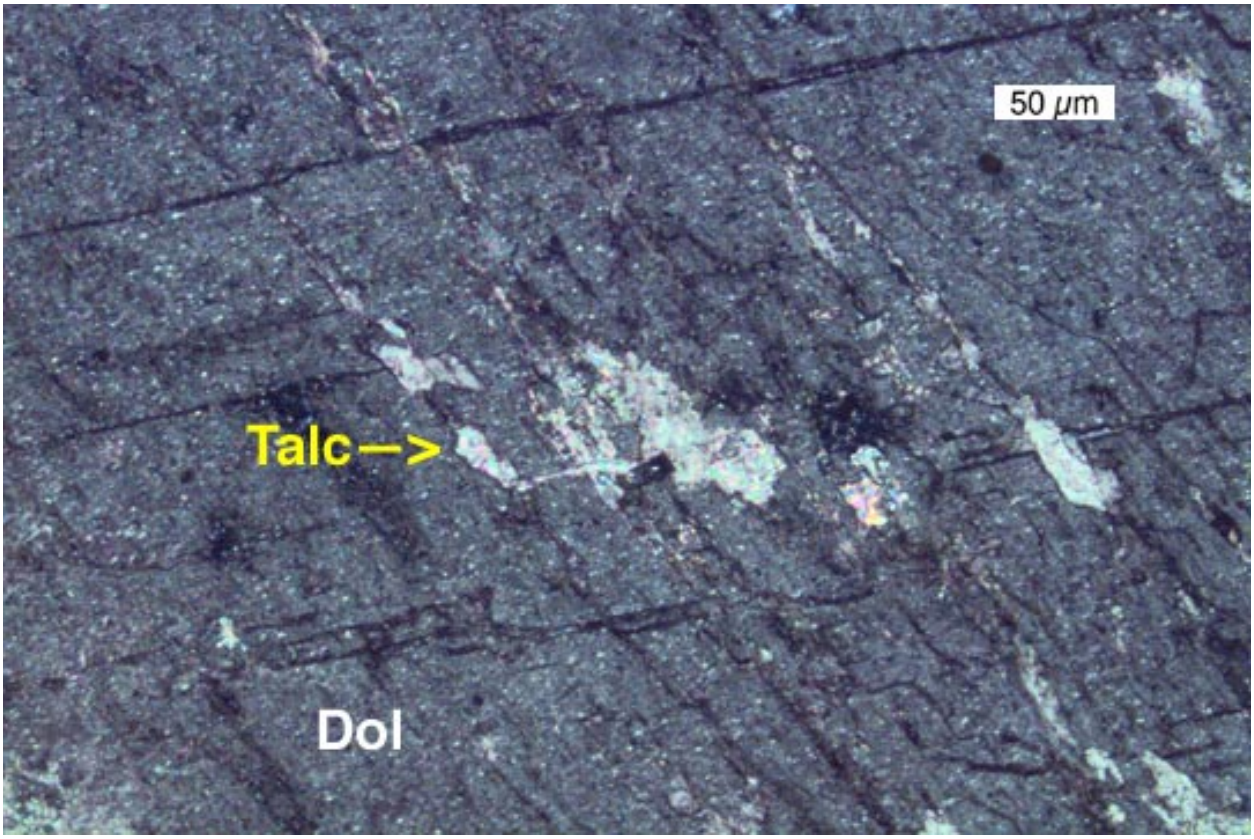

Figure 7. Photomicrograph in crossed polarized light of a large single crystal of dolomite with polycrystalline talc apparently growing along dolomite cleavage planes. Textures such as these are consistent with brittle behavior of dolomite during at least some of the talc event. This sample is from the Treasure Mine.

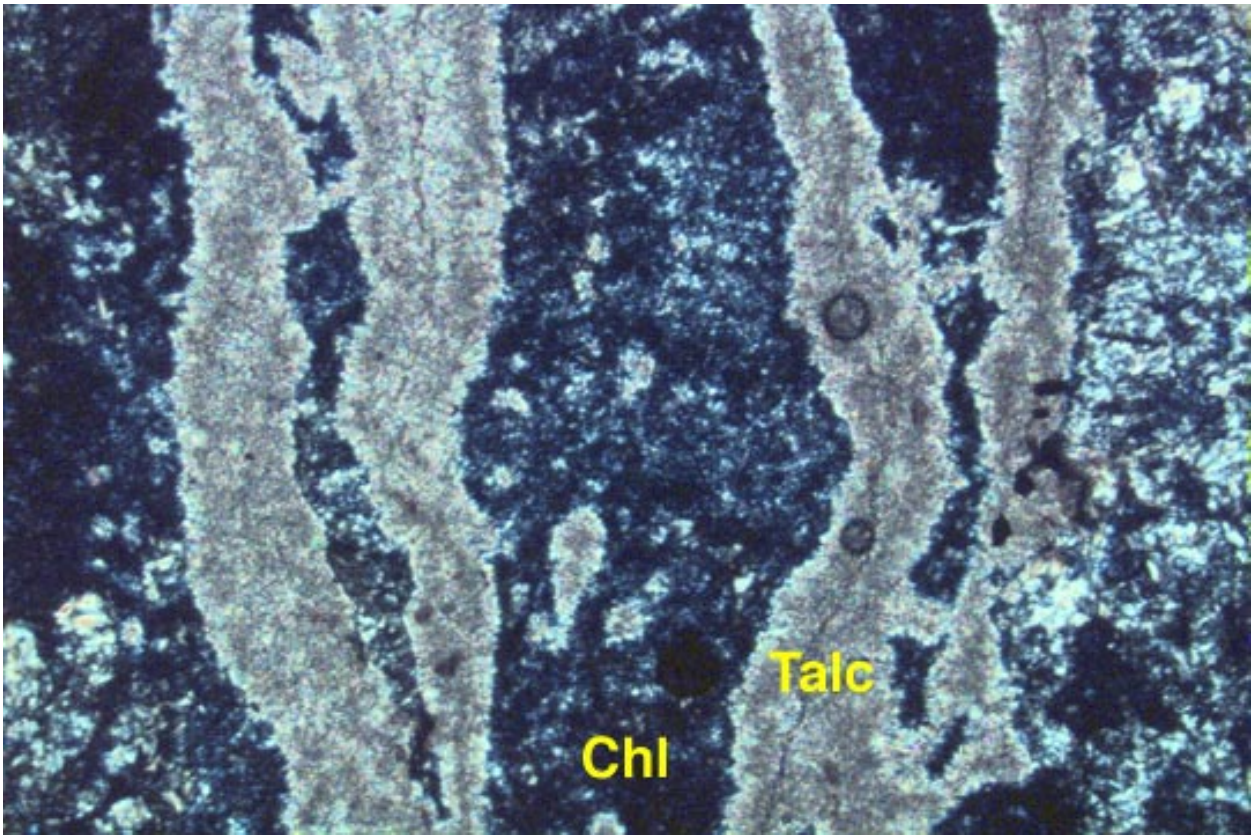

Figure 8. Photomicrograph in crossed polarized light of veins of polycrystalline talc replacing polycrystalline chlorite (Chl). Chlorite replaces quartzofeldspathic gneisses that are interbedded with marbles that have been altered to talc. Further contact with the talc forming fluids can apparently lead to talc growth from chlorite. This sample is from the Treasure Mine.

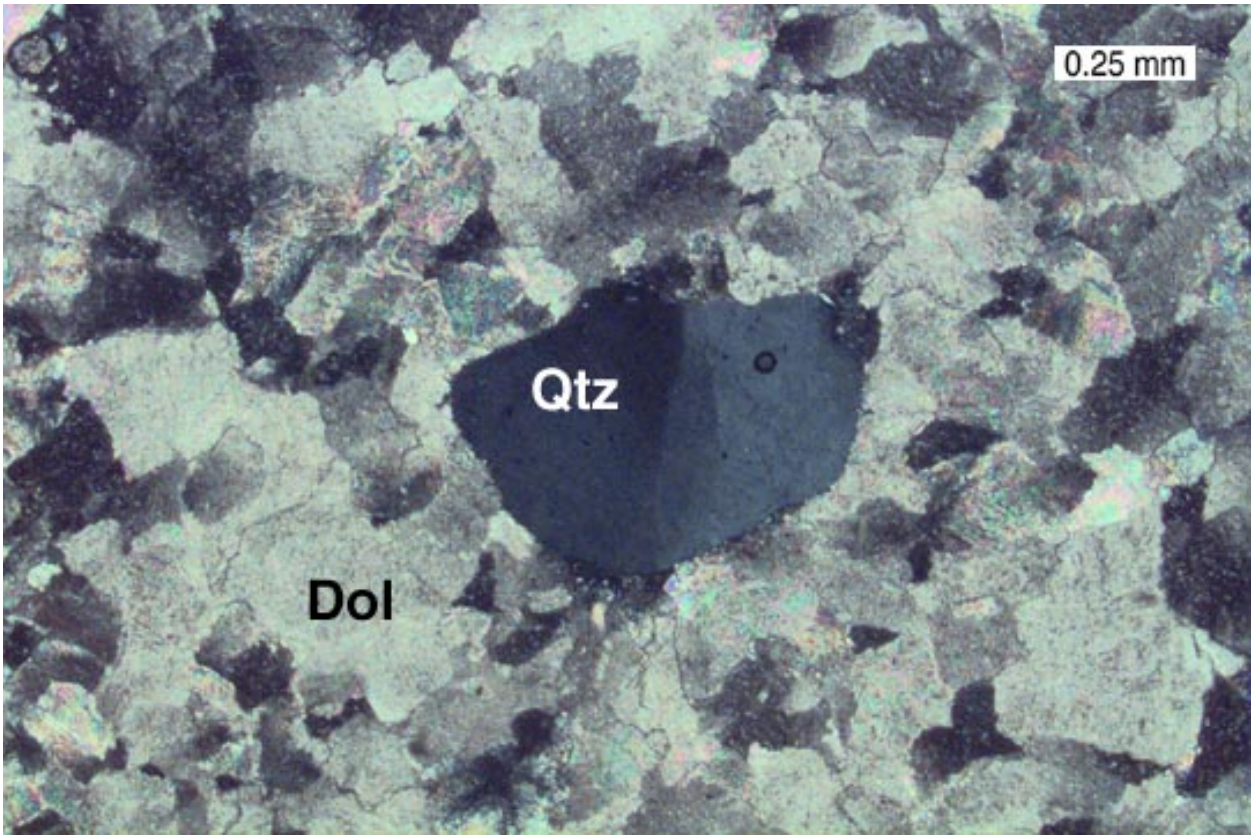

Figure 9. Photomicrograph in crossed polarized light of a single quartz grain in a dolomite marble. The quartz crystal shows undulatory extinction. No reaction between the quartz and surrounding dolomite is evident. If the quartz and dolomite were both present during upper amphibolite facies metamorphism, the quartz and dolomite should have reacted to form diopside. We believe this sample is consistent with dolomitization of calcite marbles as part of the talc-forming events that postdate regional metamorphism. This sample is from the American Chemet Mine.

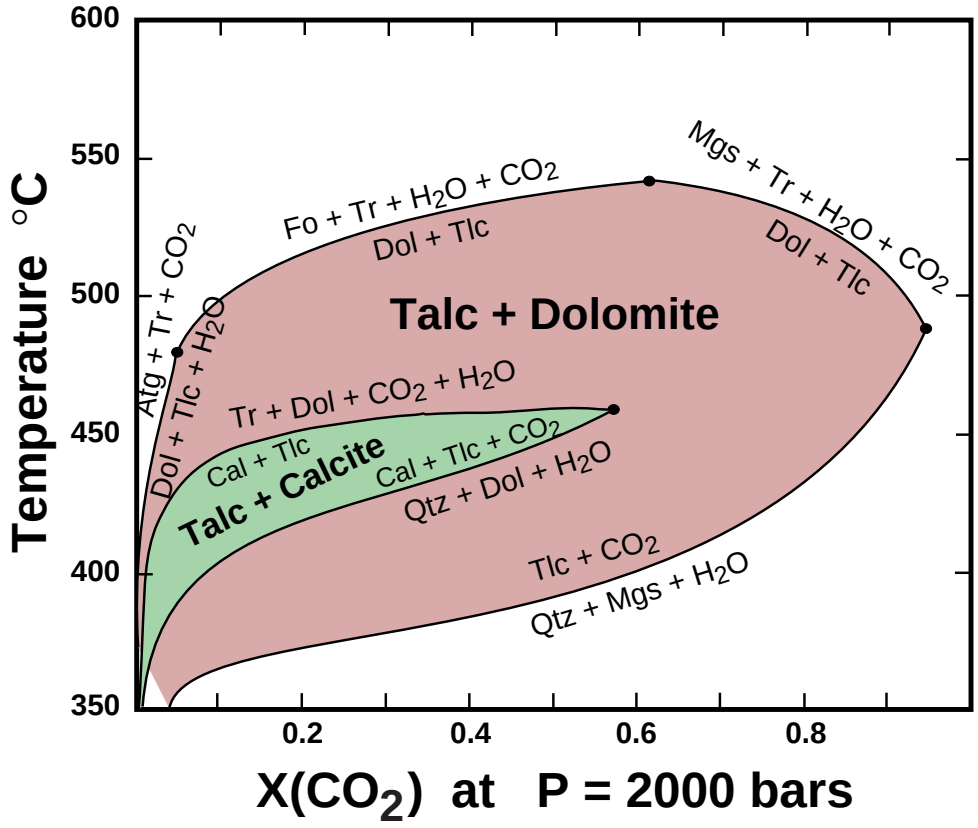

Figure 10. Stability of the assemblages talc (Tlc) + calcite (Cal) and talc + dolomite (Dol) are shown on a T-X_{CO2} diagram as calculated at 2 kb pressure by the thermodynamic model of Berman (1988). At 2 kb, talc + calcite is limited to temperatures below about 450°C and below about 0.55 X_{CO2}. Limiting reactions are shown involving the minerals tremolite (Tr), forsterite (Fo), antigorite (Atg), quartz (Qtz), and magnesite (Mgs).

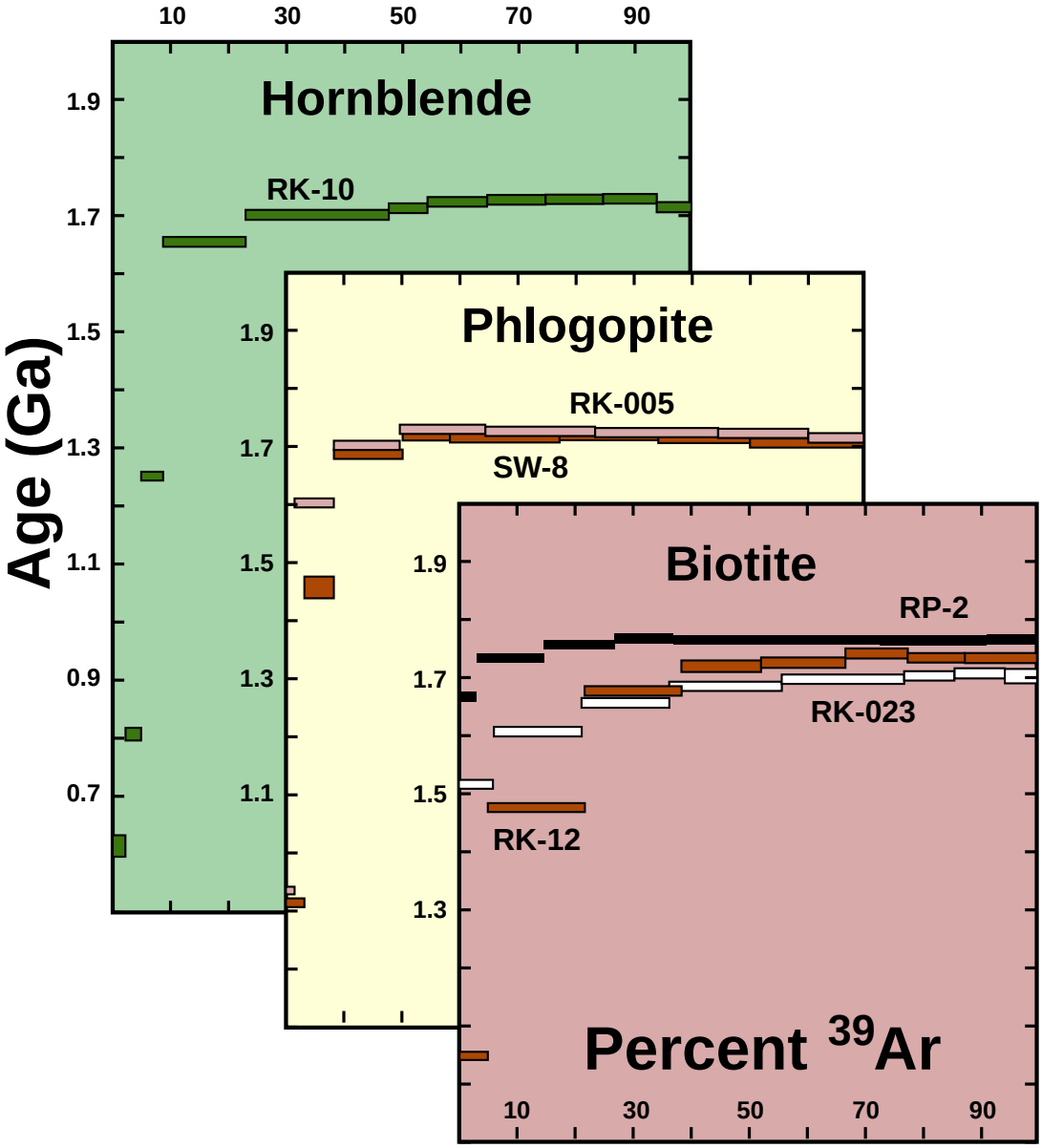

Figure 11. Argon release spectra for several micas and a hornblende from the Ruby Range. Apparent age in billions of years (Ga) is shown as a function of the cumulative percentage of ^{39}Ar released during heating steps. Sample numbers are keyed to the talc localities (see Table 1).

Sample	Mineral	Total Gas Age (Ma)	Plateau Age (Ma)
RK-10	Hornblende	1640	1725 (±13)
RK-005	Phlogopite	1700	1723 (±15)
SW-8	Phlogopite	1670	1716 (±13)
RP-2	Biotite	1757	1764 (±11)
RK-12	Biotite	1644	none
RK-023	Biotite	1659	none

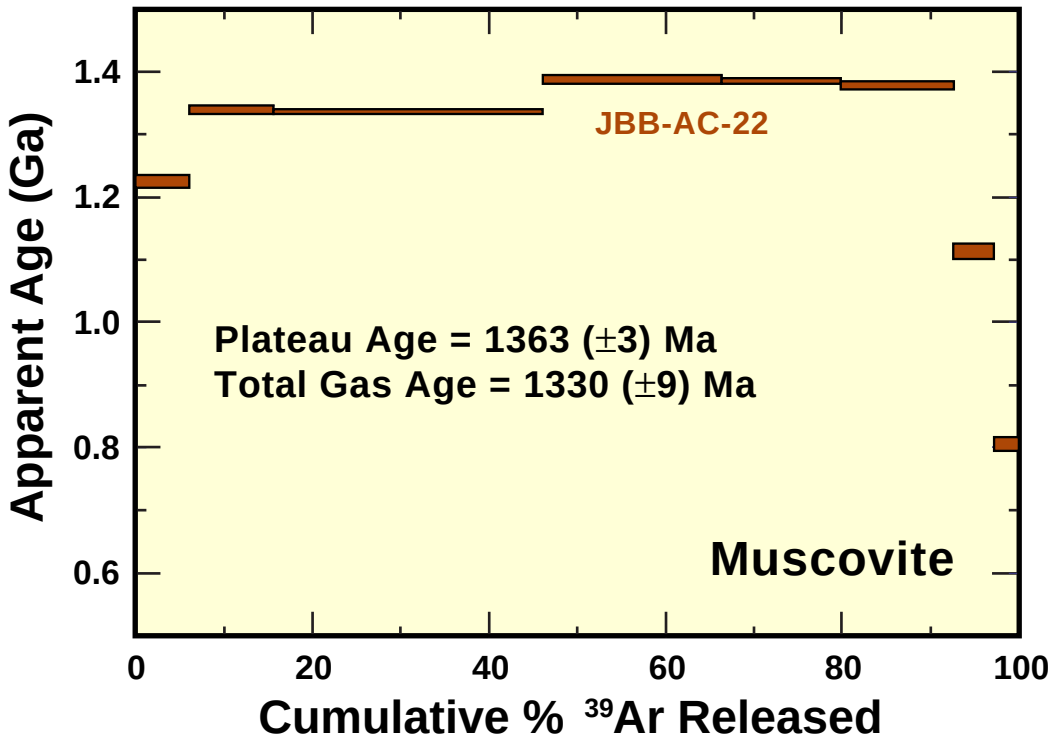

Figure 12. Argon age spectrum for a fine-grained muscovite sample from the American Chemet mine. The muscovite occurs with chlorite in an altered gneiss sample interbedded with dolomite that has been partially replaced by talc. Because the gneiss alteration is spatially and texturally associated with the talc deposits, we believe the muscovite age dates the talc formation.

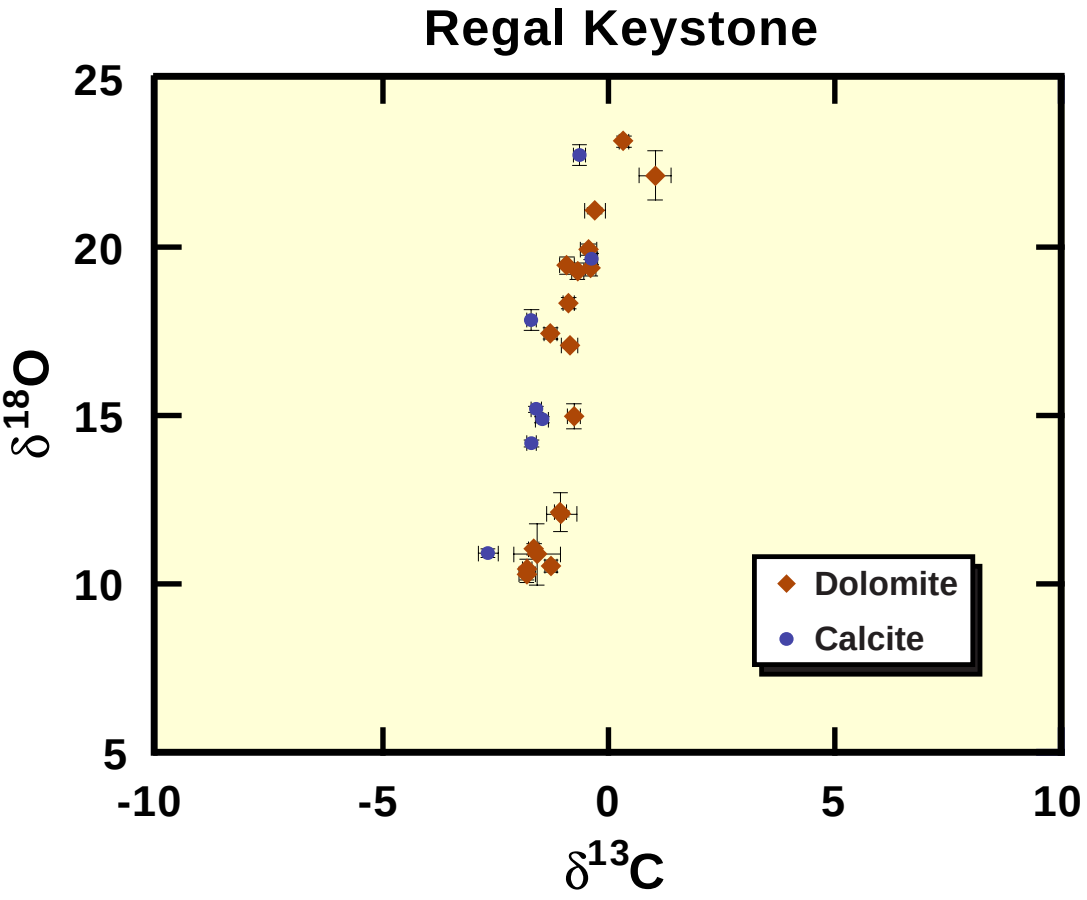

Figure 13. Oxygen and carbon isotopic values for marble samples from the Regal-Keystone Mine (Larson, 1991). Notice the great range in oxygen isotopic values and the small range in carbon isotopic values. Dolomite points are for marble samples with little or no calcite. Calcite points are for marbles that contain calcite, but may also contain dolomite. Error bars indicate the range of values for multiple measurements of the same sample.

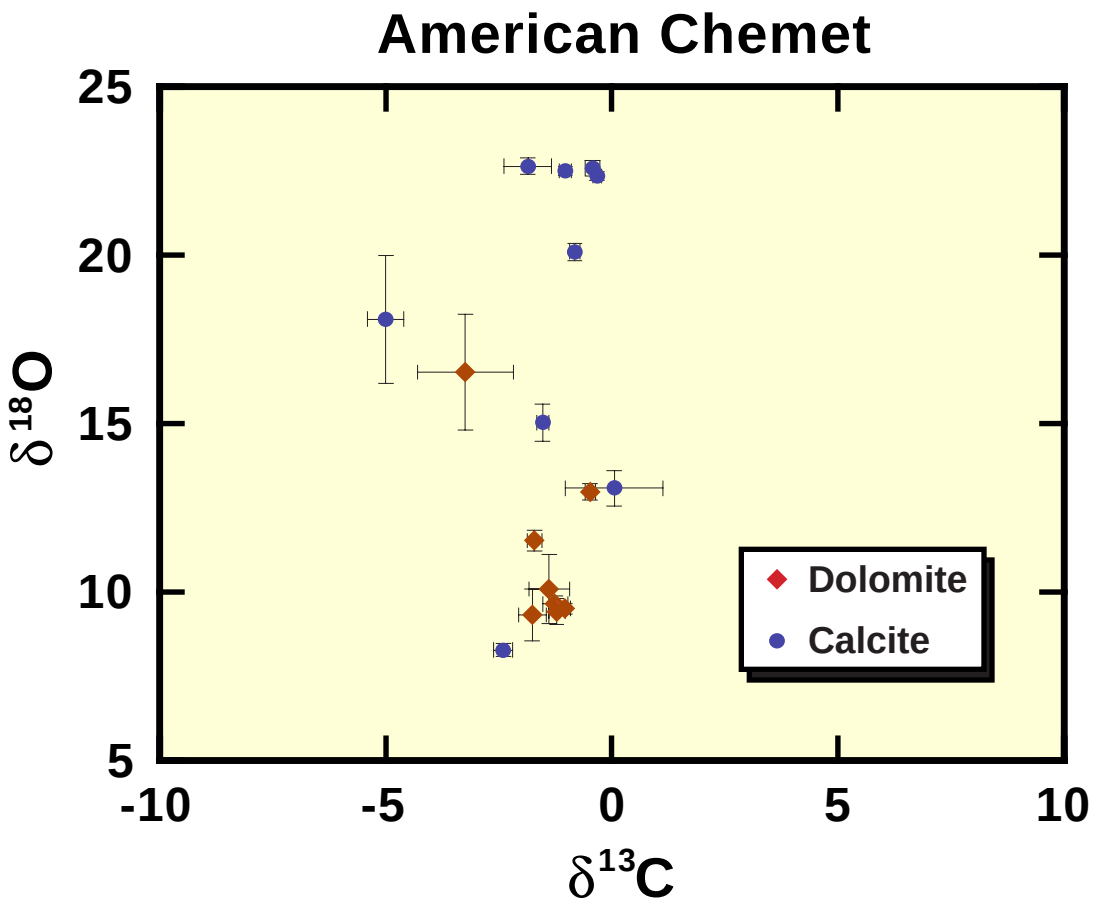

Figure 14. Oxygen and carbon isotopic values for carbonate samples from the American Chemet Mine (Vasquez, 1991). Again, notice the great range in oxygen isotopic values and the smaller range in carbon isotopic values. Dolomite points are for marble samples with little or no calcite. Calcite points are for marbles that contain calcite, but may also contain dolomite. Error bars indicate the range of values for multiple measurements of the same sample.

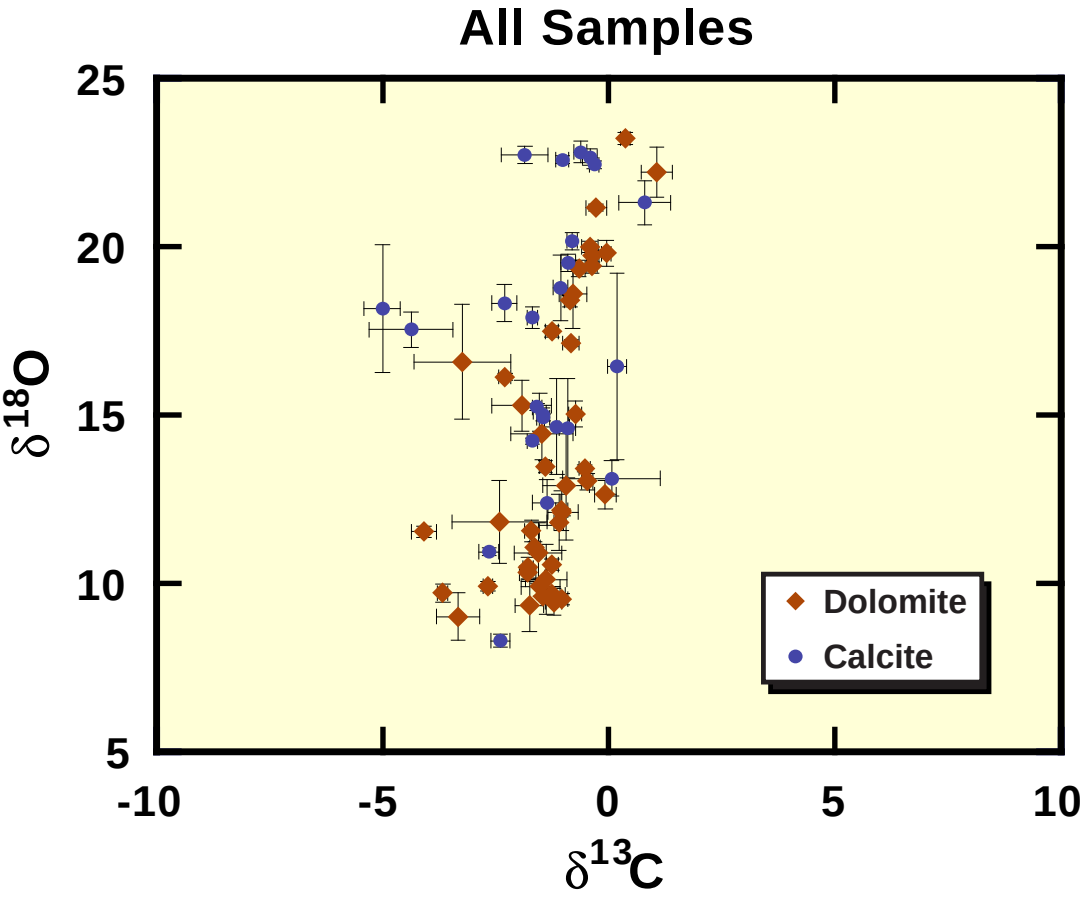

Figure 15. Oxygen and carbon isotopic values for carbonate samples from talc deposits across the Ruby Range. All of the data are consistent with alteration by a water-rich fluid that lowered the oxygen isotopic values of the carbonates, but left their carbon isotopic values relatively unchanged. Dolomite points are for marble samples with little or no calcite. Calcite points are for marbles that contain calcite, but may also contain dolomite. Error bars indicate the range of values for multiple measurements of the same sample. Large error bars for some of the samples indicate that these samples were inhomogeneous.

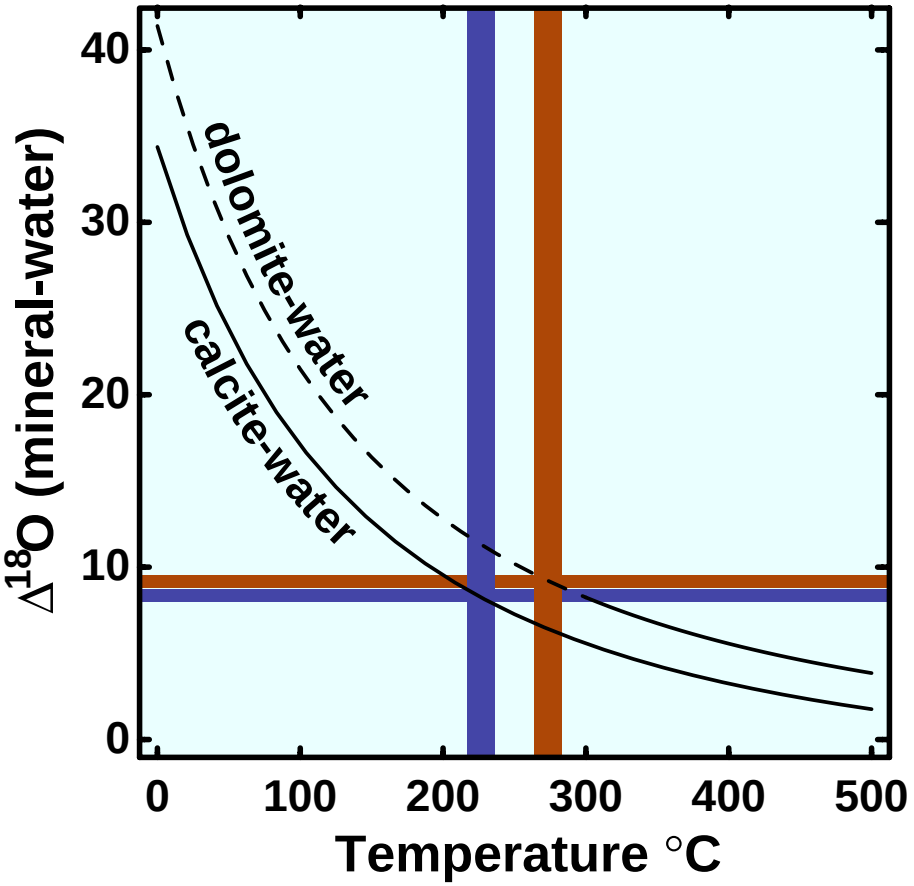

Figure 16. Oxygen isotopic fractionation curve for calcite-water as determined by Friedman and O'Neil (1977). Shown also is a calculated fractionation curve for dolomite-water, based on the calcite water curve and data for dolomite-calcite fractionation (Friedman and O'Neil, 1977). Data for the dolomite-calcite fractionation were obtained at temperatures above 300°C, hence the dashed line at lower temperatures. If the talc deposits were formed by interaction with seawater (δ^{18} O = 0), then **minimum** temperatures of talc formation can be obtained from the lowest observed oxygen isotopic values of the carbonates. The lowest calcite values (blue) give minimum temperatures of 225°C. The lowest dolomite values (brown) give minimum temperatures of 275°C.

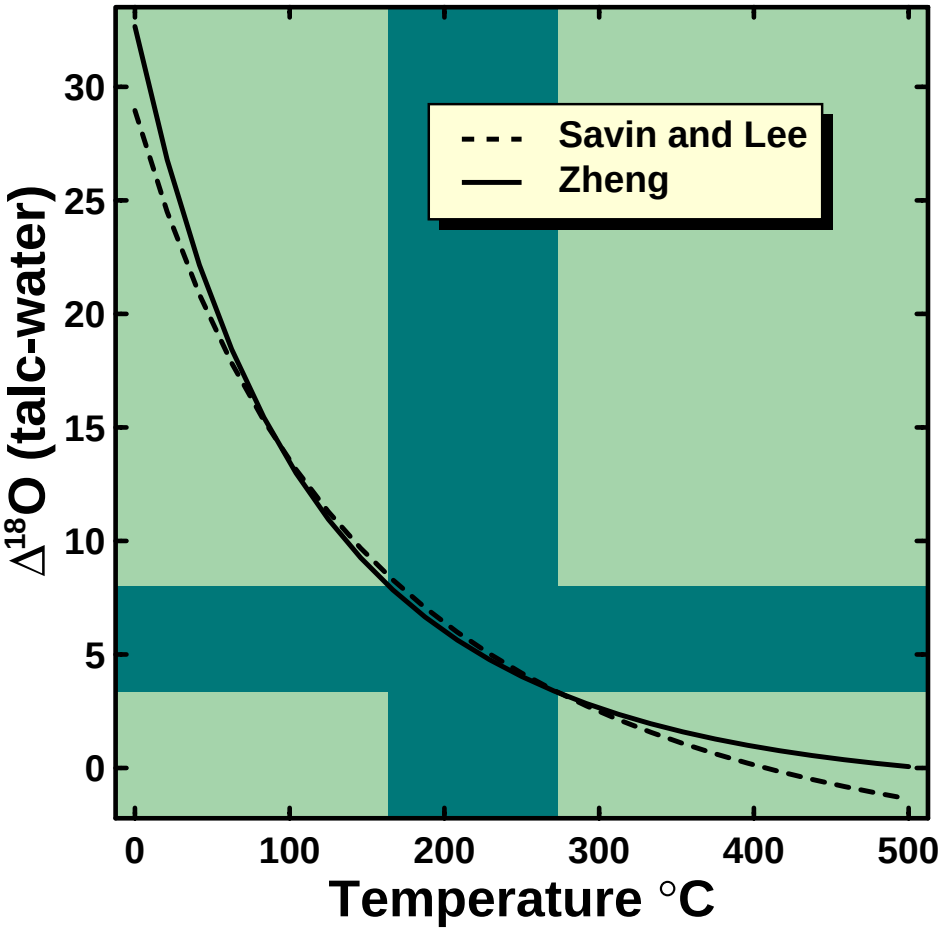

Figure 17. Theoretical oxygen isotopic fractionation between talc and water are shown as a function of temperature as calculated by Savin and Lee (1988) and Zheng (1993). The range of observed $\delta^{18}O$ values for talc when compared with seawater ($\delta^{18}O = 0$) give a range of minimum temperatures of talc formation as indicated by the dark band.

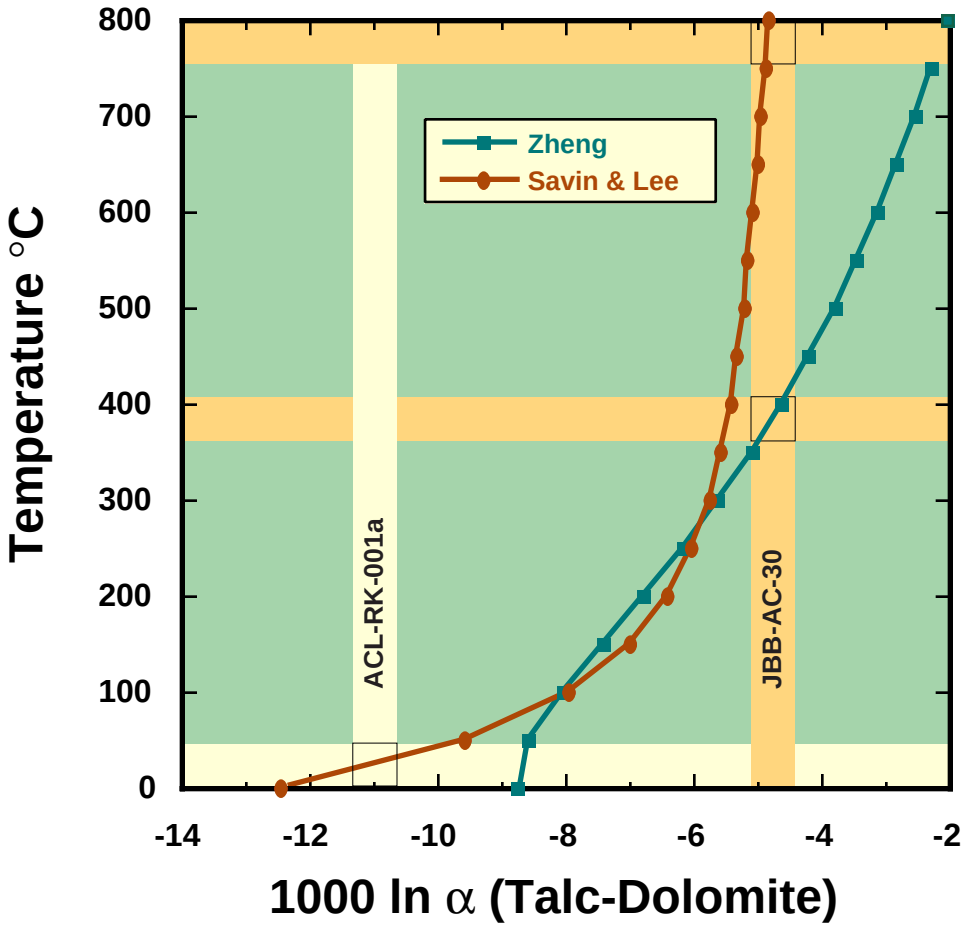

Figure 18. Oxygen isotope fractionation between talc and dolomite calculated as a function of temperature from the (extrapolated) experimental data for dolomite of Friedman and O'Neil (1977) and the theoretical models for talc of Savin and Lee (1988) and Zheng (1993). The intersections of the talc-dolomite values for two samples with the theoretical curves are indicated by black squares. The wide range of temperatures indicated by the two talc-dolomite data points are interpreted as evidence that the talc and dolomite were not in isotopic equilibrium.

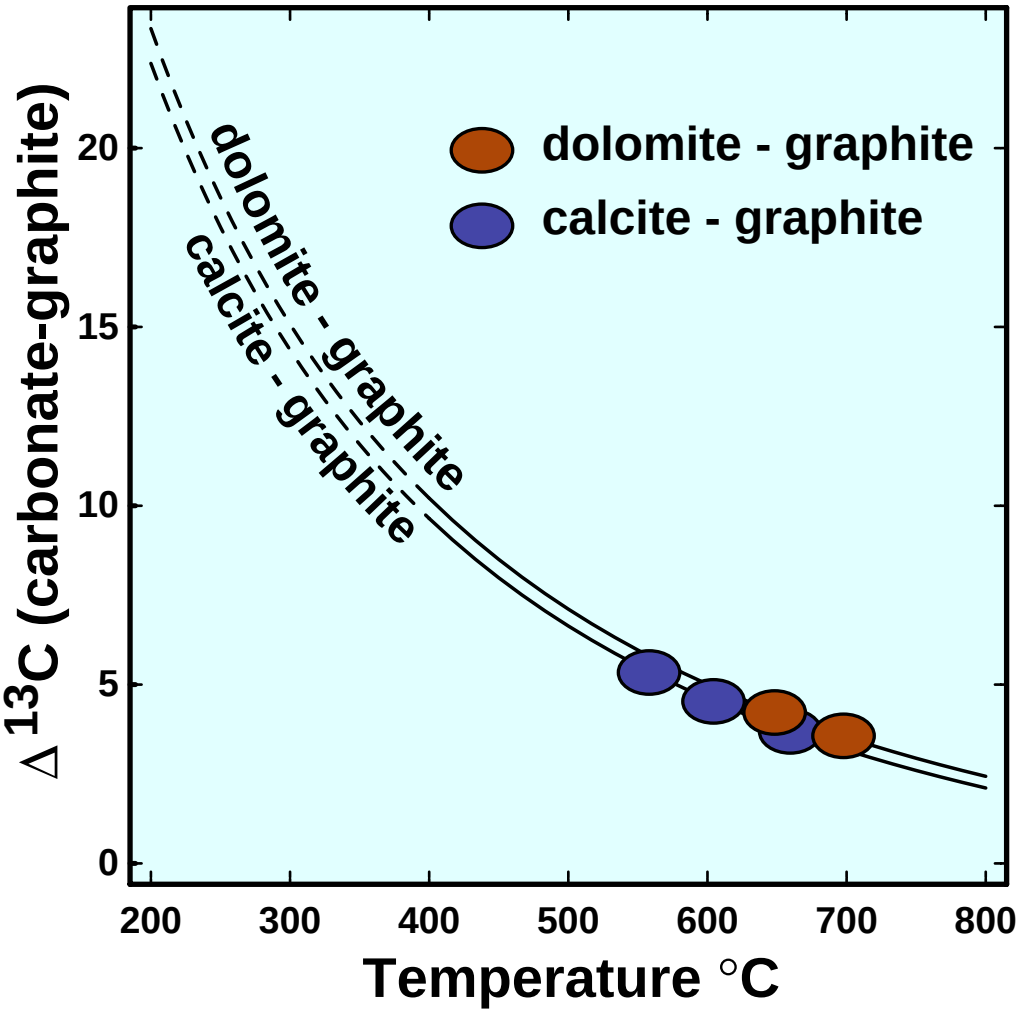

Figure 19. The temperature variation of the carbon isotopic fractionation between calcite and graphite as calibrated by Dunn and Valley (1992). Data from Table 3 for cabonate-graphite pairs are shown on the appropriate fractionation curve based on their $\Delta^{13}C$ (carbonate-graphite) values. Observed fractionation for Ruby Range samples appears to record upper amphibolite facies temperatures even though the oxygen isotopes for the calcite samples have been reset at lower temperatures. These data are consistent with our suggestion that the talc-forming fluid was poor in CO_2 and rich in H_2O. One data point (JBB-AC-22) is not shown because its low $\Delta^{13}C$ value (1.3) is beyond the range of the calibration and would yield unreasonably high temperatures.